Modelling the effects of lymph node swelling on T-cell response

Sarah C Johnson[1], Jennifer Frattolin[1], Lowell T. Edgar [1], Mohammad Jafarnejad[2], James E. Moore Jr.[1]

1 Department of Bioengineering, Imperial College London, London, United Kingdom

2 Department of Biomedical Engineering, Johns Hopkins University School of Medicine, Baltimore, MD, USA

* james.moore.jr@imperial.ac.uk

Abstract

Swelling of the lymph nodes is commonly observed during the adaptive immune response, yet its impacts on T cell trafficking and subsequent immune response are not well known. To better understand the effect of macro-scale alterations in the lymph node, we developed an agent-based model of the lymph node paracortex, describing T cell trafficking and response to antigen-presenting dendritic cells alongside swelling-induced changes in T cell recruitment and egress, and regulation of expression of egress-modulating T cell receptor Sphingosine-1-phosphate receptor-1. Validation of the model was achieved with *in-silico* replication of a range of published *in-vivo* and cell culture experiments. Analysis of $CD4^+$ and $CD8^+$ effector T cell response under varying swelling conditions showed that paracortical swelling aided initial T cell activation but could inhibit subsequent effector $CD8^+$ T cell production if swelling occurs too early in the T cell proliferative phase. A global sensitivity analysis revealed that the effects of some parameters switch from aiding to inhibiting T cell response over a ten day response period. Furthermore, temporarily extending retention of newly differentiated effector T cells, mediated by Sphingosine-1-phosphate receptor-1 expression, mitigated some of the effects of early paracortical swelling. These results

suggest that targeting the timing of lymph node swelling and temporary effector T cell retention may offer new ways to manipulate immune response.

Author summary

Within the lymph nodes the interaction of T cells and antigen presenting cells play a crucial role in initiating the adaptive immune response, resulting in effector T cells that travel to the infection site. Accompanying swelling of lymph nodes is commonly observed, yet the impact on T cell trafficking through the node and the subsequent immune response are not well known. We developed a novel agent-based model of a lymph node, describing immune response-induced expansion, contraction and changes in T cell recruitment and egress. We also describe the regulation of T cell expression of the Sphingosine-1-phosphate receptor-1, which is known to play an important role in T cell trafficking. We found that although swelling aids T cell activation, too early an increase in paracortical volume hinders the CD8+ effector T cell response. We also found that temporarily maintaining the down-regulation of Sphingosine-1-phosphate receptor-1 expression on newly differentiated effector T cells greatly increased the overall effector T cell output, and could counteract the loss in effector TC production due to early swelling. Our findings suggest that targeting the timing of lymph node swelling and temporary effector T cell retention may offer new ways to manipulate immune response.

Introduction

The lymphatic system is a converging network of organs and lymphatic vessels (LVs) that maintains fluid balance in the body and also delivers crucial antigen information to lymph nodes (LNs) for initiation of adaptive immunity. A successful immune response relies not only on the interaction of different immune cell types, but also on the maintenance of an appropriate physical environment in the LNs to facilitate those interactions. LNs contain specific compartments populated by T cells (TCs), B cells, fibroreticular cells (FRCs), some of which are lined by lymphatic endothelial cells (LECs) [1, 2]. When antigens are presented (either suspended in lymph or as captured by incoming antigen presenting cells), the LNs physical environment change over time.

Swelling of LNs is a well-known consequence, but the effects of swelling on the processes crucial for adaptive immunity are not well understood.

Expansion of LNs depends on the presence and activity of Dendritic Cells (DCs), B cell signalling and TC residence time in the LNs [3–5]. In the initial days, TC exit rate falls, blood flow to the LNs increases, and inflammatory signalling results in a 3-5 fold increase in TC recruitment [6–8]. Mass of LNs increases 2-5-fold, accompanied by a similar increase in cellularity, while in the first 48-96 hours, the FRCs elongate, allowing accommodation of increases in the size of the LNs [9–11]. Proliferation of stromal cells lags behind the increase in immune cells but subsequent proliferation of LECs and FRCs allow maintenance of the LNs architecture during further expansion [5, 11, 12]. The blood vessels of the LNs also grow, increasing blood vessel volume roughly proportional to overall volume of the LNs, accompanied by further TC recruitment [4, 7, 13].

Between 2 and 5 days post-immunisation, the number of antigen-presenting DCs in the LNs peaks, TC activation and proliferation is underway and TC egress increases 3-6 fold [5, 9, 14, 15]. Expansion of the medullary and SCS areas has also been observed, which aids in the increase in TC egress rate [16]. Recruitment of TCs then declines, HEV, FRC and TC proliferation subsides, remaining effector TCs may undergo apoptosis and the LNs return to their baseline volume [13]. Following a primary response, FRC, LEC and blood vessel endothelial cell numbers remain elevated within denser LNs structures for at least a month [12].

To pass through these phases, the underlying antigenic simulation must be sufficient to trigger lymphocyte retention, activation and proliferation while a successful immune response occurs when TCs further differentiate into effector cells and migrate out of the LNs [17]. Migrating DCs cross the SCS floor in a chemokine and integrin-aided fashion and migrate into the paracortex [18]. TCs and B Cells mainly enter the LNs by transmigrating from blood vessels in the paracortex [19]. Typically 1 in 10,000 TCs express a complementary TC receptor to the antigen fragment presented by DCs within a MHCI (to $CD8^+$ TCs) or MHCII ($CD4^+$ TCs) molecule [20, 21]. Naive cognate TCs initially make short contacts with DCs, but after around 8 hours, progress to longer interactions (>1hr) before returning to short interactions as TCs activate and divide [22]. With sufficient affinity and stimuli, TCs undergo activation, secrete inflammatory and activation-facilitating cytokines [23]. Some TCs differentiate into

effector TCs and up-regulate the Sphingosine-1-phosphate receptor-1 ($S1P_1r$) facilitating egress [24]. An increasing proportion of TCs differentiate into memory cells [25, 26]. Proliferation of $CD8^+$ TCs can continue independent of further stimuli, possibly with an impaired memory cell response [27, 28]. Contrastingly, $CD4^+$ TCs are more dependent on sustained inflammatory stimulation for continued differentiation [29]. As infectious signals subside, remaining effector TCs undergo apoptosis while memory cells go into circulation [30].

Throughout these processes, the egress of TCs from the LNs is modulated by Sphingosine-1-Phosphate (S1P) and chemokine signalling axes. After entering the LNs, TCs initially express $S1P_1r$ at very low levels but begin re-expressing $S1P_1r$ after 2 hours [31, 32]. TCs exit the LNs by probing and subsequently entering cortical sinuses in the paracortex or the interface with the medulla, aided by chemotaxis as both destinations contain higher S1P concentrations (Fig 1A) [33, 34]. During inflammation, TC $S1P_1r$ expression is reciprocally regulated by CD69, an early TC activation marker that can be up-regulated in TCs by the presence of inflammatory mediators, contributing to the initial decrease in TC egress and later retention of activated TCs [35].

Fig 1. The structure of the LN and the ABM geometry. (A) LN structure displaying the pathway of arriving lymphatic fluid. (B) The model describes a spherical paracortex, TCs enter in the center and exit near the interface with the medulla and SCS. The paracortex radius expands as a function of TCs present. (C) TCs move to adjacent grid-compartments, interact with neighbouring agents and are influenced by the grid-compartment properties, which are updated each time-step. Micro-scale signals can influence recruitment, exit and DCs interaction. (D) Macro-scale changes in paracortex size influence TC recruitment and exit rate. (E) Micro-scale and macro-scale changes influence each other and affect the number of TCs present

The exploration of potential roles for swelling of LNs in adaptive immunity is limited by the range of possible experiments in which parts of the process could be modulated, and the ability to track relevant outcomes in real time. Mathematical models can help fill these knowledge gaps, and suggest new experiments that target specific mechanisms and measure outcomes at specific time points. Modelling cell populations with partial differential equations is computationally expensive and typically involves assuming uniform cell responses to stimuli. Within Agent Based Models (ABMs), cells are described as discreet, and by modelling the interaction of thousands of agents behaving individually, it is possible to capture emergent behaviour. The TC immune response in

an expanding paracortex has previously been described with an ABM, however the assumption of a constant TC occupancy of the total paracortical volume potentially neglected the effects of crowding on cell migration [36–38]. ABMs of fixed-volume LNs have provided insight relevant to vaccine design, for example to investigate the effect of antigenic peptide separation from MHC molecules on TC activation, influential aspects of TC-DC interaction, and effector TC or memory cell production [39–43]. Simulations integrating a fixed-volume hybrid lattice-based model and a continuous model allowed incorporation of chemokine diffusion with TC, B cell and DC interactions in the LNs. This showed that both early antigen removal and regulation of TC exit affected the balanced system dynamics, indicating that macroscale swelling is likely to significantly affect micro-scale TC activity [44]. Indeed, models of lymph flow through the LNs suggest that altered oncotic and medulla pressure alone would dramatically alter cell, cytokine and chemokine distribution [45, 46].

In summary, the adaptive immune response involves careful trafficking and coordination of immune cell movements in the LNs, suggesting that swelling of LNs is likely to significantly impact the adaptive response at the micro-scale. To investigate this hypothesis, a computational ABM was developed that incorporates TC and DC dynamics, swelling of LNs and changes in TC recruitment and egress. The model was first validated against the available experimental data. The results suggest an important role for swelling of LNs in TC population dynamics.

Materials and methods

ABM Geometry

The paracortex is modelled as a sphere with initial radius R_0=400μm, derived from confocal images [2, 47]. The modelling domain is divided into cuboid grid compartments, edge length of 6μm (Fig 1C). To reduce computational expense, geometric symmetry is assumed so that only one-half of the total spherical geometry is modelled. Variables for each compartment determining features such as 'exit' or 'boundary' are stored in a parallel 'ValueLayer'. Paracortical volume is calculated as a function of TCs present and paracortical swelling, and contraction is achieved by changing the type of region

that each grid compartment represents, while maintaining entry and exit areas defined as a percentage of the outer radius (Fig 2A,G).

Fig 2. Grouping the parameters of the model. Model geometry, TC initialisation, DC initialisation and T cell movement are not varied in the sensitivity analysis. TC movement parameters were varied in preliminary trials before being fixed. Reference sources for all parameters are available in S2 File.

TC recruitment

Under baseline conditions, TC recruitment rate was specified as 2000 TCs/hour, naive TC transit time (T_{res}) as 6-24 hours and the TC-to-compartment ratio was assumed constant (see S1.1). In accordance with images depicting HEV location, 90% of TCs enter at 'HEV entry' compartments designated as the inner half of the paracortical radius [48]. These grids also correspond to the blood vessel volume (V_B), which changes in proportion to overall paracortical volume change [4, 45]. Remaining TCs enter via the SCS interface at compartments adjacent to the afferent half of the external surface. To allow blood vessel volume (V_B) changes to contribute to TC recruitment rate, TC influx is made proportional to normalised blood vessel volume $\bar{V_B}$ (normalised with respect to the pre-stimulus value). Acute recruitment changes due to inflammation-induced signalling cascades at the HEVs are represented by incorporating an inflammatory index, (I_f), triggered by antigenic presence (sum of MHC thresholds to trigger (T1) and cap (T2) recruitment)(2). TC influx is therefore :

$$T_{in}(t) = \frac{N_T}{T_{Res}} \quad I_F(t)\bar{V_B}(t) \tag{1}$$

Where N_T is the initial number of TCs present. Threshold values T1 and T2 were estimated from *in-vivo* observations of stimuli application and recruitment response.

$$I_f(t) = \begin{cases} 1 & \sum_{n=1}^{N_{DC}} MHC_n(t) \leq T1 \\ 1 + R_F \sum_{n=1}^{N_{DC}} MHC_n(t) & T1 \leq \sum_{n=1}^{N_{DC}} MHC_n(t) \leq T2 \\ 1 + R_F T2 & \sum_{n=1}^{N_{DC}} MHC_n(t) \geq T2 \end{cases} \quad (2)$$

TC egress and S1P$_1$r expression

The relative expression of S1P$_1$r (SP) is varied from 0.01 (egress inhibition) to 1.4 (egress facilitation). Following TC entry into LNs, S1P$_1$r is down-regulated for 45-180 minutes, with SP=0.1 (Fig 2F) [32]. TCs undergo inflammation-induced S1P$_1r$ inflammation, to reflect the 3-30 fold decrease in TC egress in the initial 24 hours of an immune response [49]. This is implemented when the antigenic presence (represented by total MHCII present) first exceeds the equivalent of 240 agDCs. Activation-induced TC S1P$_1$r down-regulation and subsequent re-expression as TCs undergo differentiation is applied by decreasing SP when TCs first become activated, increasing SP as TCs differentiate into effector TCs, and further increasing SP when effector TCs undergo >= 7 divisions [31, 50, 51].

TC and DC motility and interaction

DCs are modelled as 6μm diameter spheres, but interact with up to a user-defined maximum number of TCs at one time (B$_{max}$), within a two grid radius, to reflect long dendrites (Fig 2B). Interaction times are drawn from a Weibull and two uniform probability distributions, with brief 3 minute interactions for non-cognate TCs (T$_{NC}$). Cognate TCs initially undergo short (T$_{short}$) interactions, of 10-15 minutes, then proceed to longer interactions (T$_{long}$) of 50-70 minutes (Fig 2E). Each agDC presents a decaying MHCI and MHCII signal (Eq.S1) with half lives MHCI$_{\frac{1}{2}}$ and MHCII$_{\frac{1}{2}}$, obtained from *in-vitro* labelling of MHC molecules presented on DCs [52–55].

TCs (70% Helper TCs (CD4$^+$) and 30% cytotoxic (CD8$^+$ TCs) are modelled as spheres of radius 3.2μm that initially occupy 60% of the total paracortex volume [56].

Each 20 second time-step TCs are permitted to move, with probability β, one grid length to a random available neighbouring grid compartment, where availability is governed by crowding parameter γ. The proportion of cognate TCs recruited each time-step (F_{cog}) was obtained from reported *in-vivo* frequency of antigen-specific TCs [21].

Cognate TCs gain 'stimulation' (S) during interactions with agDCs at rate K_s, proportional to MHC presented, while losing stimulation at rate λ_S (Fig 2C), similarly to the methods of [37, 41, 57]. Probability of subsequent activation and differentiation depends on accumulated stimulation. More simulation was required to activate $CD8^+$ TCs with the same probability as $CD4^+$ TCs. However, if the DC is 'licenced', which occurs post-interaction with an activated $CD4^+$ TC, $CD8^+$ TC and $CD4^+$ TC stimulation requirements are equal. This is to reflect facilitated $CD8^+$ activation as a result of activated $CD4^+$-induced production of cytokines [58]. The fraction of effector TCs that differentiate into memory TCs increases from 0.01 to 0.04 as TC progress from 'early effectors' (< 6 proliferations) to 'late effectors' [59]. See S1 File for full rules and S2 File for parameter references.

Simulations and analysis

The ABM was built in RepastSimphony (http://repast.sourceforge.net) as a class based model (S1 Fig) written in java with repeated rules each timestep (Fig 3. Further UML-based descriptions are available within S3 File. The Imperial College High Performance Computing cluster was used to carry out batch simulations and data analysis was carried out in Matlab. Complete code is available at github.com/johnsara04/paracortex_model_johnson19. Raw data is available at [xxx].

Fig 3. Setup processes in the model. (A) Individual agents, (TCs and DCs) store variables regarding their history and present state while 'projections' between agents allow information transfer. The model is equilibrated then volume change is introduced and initial volumes re-initialised. There is discernment between TCs that enter and TCs present from time 0. Each time step represents 20s of simulated time and model outputs are recorded every, 1, 15 or 180 time-steps dependent on user specification. (B) The repeated sequence of sub-methods that make up the 'main' process. Each method () contains further rules and actions, with descriptions available within the supplementary S3 File.

Baseline simulations with limited paracortical swelling (V_{Max}) were performed to ensure estimated parameters (listed in S2 File) produced realistic TC response dynamics. TC response was then assessed while varying maximal fold-increase in swelling volume (V_{Max}) from 1 to 2.8, varying the required number of TCs present to reach half V_{Max}, (T_{mid}) between 8e4 and 13e4 and modulating $S1P_1r$ expression on newly differentiated TCs (effector TCs having undergone 4-6 proliferations). Effector TC response was assessed when TCs were permitted to re-enter HEVs and also when increasing exit probability if two TCs occupied an exit compartment. Analysis of correlation was assessed by calculating Pearsons's coefficient, ANOVA was applied to detect variance, and linear regression was used to confirm linear relationships. A significance threshold of $p<0.05$ was used throughout.

A global sensitivity analysis was also carried out using 300 parameter combinations, repeating simulations with each combination 3 times. Combinations were selected using Latin Hypercube sampling, to reduce sample size while ensuring inclusion of samples near the minimum and maximum parameter ranges. Partial-rank correlation coefficients were calculated between each parameter and output of interest (activated TCs, effector TCs, memory TCs, effector TCs exited and memory TCs exited) from day 3 to 13, assuming monotonic relationships [60].

Validation

The relationship between initial proportion of cognate TCs and subsequent effector TC production has been studied *in-vitro* by applying antigen to pools of TCs with known starting cognate frequencies [59,61]. To compare the model behaviour, the initial proportion of cognate TCs was varied *in-silico* between $1.0x10^{-5}$ and $1.4x10^{-4}$ and the resulting $CD4^+$ and $CD8^+$ effector TC response compared to the *in-vitro* results. The

effect of varying stimuli strength on $CD8^+$ effector TC response in LNs has been investigated *in-vivo* and *in-vitro* by varying injecting mice with varying bacterial antigen dose or agDCs and applying antigen-pulsed DCs to TC culture [62, 63]. These experiments were replicated *in-silico* by varying agDCs as a fraction of total TCs (ϕ_{DC}) incrementally from 0.04 to 0.0015 (2200 to 77 agDCs), and comparing $CD8^+$ TC response. The effect of curtailing the duration of antigenic stimuli has been carried out in rat LNs by injecting diptheria toxin (DT)-sensitive agDCs into the LNs then eliminating the DCs with DT injection, prior to natural DC apoptosis [64]. Early DC apoptosis was simulated *in-silico* and the effect on the total number of $CD8^+$ effector TCs compared to the published *in-vivo* observations. Finally, down-regulation of $S1P_1r$ on activated TCs was abolished *in-silico* and total activated and cognate $CD4^+$ and $CD8^+$ TCs present compared to similar experiments [32, 65].

Results

The model produces realistic baseline TC motility and response to agDCs

The average TC velocity (n=200) was 13.1μm/min and reached 24μm/min (Fig 4D), in-line with murine *in-vivo* measurements [48, 66–69]. TC displacement scaled well with the square root of time, (Fig 4E,F) indicating random walk behaviour and the motility coefficient (CM) was 63.2μm/min, which is within the range of 50-100μm/min observed in mice [70]. The mean TC paracortex transit time was 13.1 hours (n=16,000), ranging from 20 minutes to >60 hours (Fig 4C), in-line with observations that 74% of $CD4^+$TCs and 64% of $CD8^+$ TCs transit the murine LNs within a day [71].

Fig 4. Baseline TC motility. (A) TC tracking through the paracortex with individual tracks displayed. TCs entered centrally, representing entry from HEVs, and at the top of the paracortex, representing entry in afferent lymph (yellow arrow). TCs exited at the periphery (green arrows). (B) Tracks of TCs (each colour represents one TC path) transposed to the same origin point dis- play the random walk behaviour outwards from the origin. (C) Most TCs completed transit in <24hrs. (D) Mean velocity of TCs. (E) Mean and SEM (n=100) of TC displacement from entry point. (F) Mean (+/-SEM) of TC displacement showed a linear relationship to the square root of time.

TC responses to AgDC stimuli corresponded well to experimental data from cell-culture models and *in-vivo* trials in mice, sheep and rats, displaying the expected phases of TC trafficking and response (S2 Fig). TC numbers began to increase around 6 hours after initial agDCs entry, and by day 11 had returned to within 15% of pre-stimulus values (Fig 5A), in-line with temporal responses observed *in-vivo* [9, 14, 72]. The appearance of activated, effector, and memory TCs began at 16-24 hours, day 3.5 and day 5 post-agDC entry, respectively, in agreement with cell-culture models and in-vivo observations [73, 74]. Effector $CD4^+$ TCs appeared 1-1.5 hours before $CD8^+$ effector TCs (Fig 5A,B). As observed in studies using cell culture, the peak population of cognate $CD8^+$ TCs was an order of magnitude higher than that of $CD4^+$ TCs (Fig 5C) [75]. The contraction phase began at day 7 and continued through day 11. The increase in TC egress rate peaked a day later than the increase in TC entry rate (Fig 5D), corresponding well with *in-vivo* observations of delayed increase in TC egress and TC recruitment dynamics [10, 76].

Fig 5. TCs response in the paracortex following entry of agDCs. Average result with SEM of 12 simulations. AgDCs are depicted as dot-dashed line in B. The total number of TCs (black line in A) peaked in the paracortex at 3.5 days, and was comprised mainly of non-cognate naïve TCs, as the number of effector TCs (blue line A) peaked at day 6. This contributes to the second peak in the total TC number. The number of activated TCs (red line in B) began 12 hours after the first agDCs entered. Memory TCs (black line in B) began to appear at 5 days and 25% of the peak number of memory TCs remained at the end of the simulation. Cognate $CD4^+$ TCs (Green line in C) began to proliferate extensively at day 2.2, compared to cognate $CD8^+$ TCs (purple line C) that began to proliferate at day 4 and reached numbers 10x more than cognate $CD4^+$ TCs. D. TC entry rate increased 2x due to detection of antigenic stimulus whilst TC egress rate declined between day 1 and 2, then increased 3x by day 4.

When the proportion of initially cognate TCs, F_{cog}, was increased from 7e-5 to 13e-5, total cognate $CD8^+$ TC number increased by 56% (S3 FigF), comparing well to the 62% increase observed *in-vivo* [59]. Simulations across a wider range of F_{cog} values confirmed a monotonic trend (S3 FigC). Simulations designed to replicate *in-vivo* experiments [61] showed $CD4^+$ numbers generally increasing with F_{cog}, but a slight decrease at F_{cog}=1.6e-6 (Figure S3B). Further simulations at higher values of F_{cog} predicted a trend of increasing cognate $CD4^+$ TC numbers, consistent with the *in-vivo* observations (S3 FigD).

Increasing the percentage of agDCs,ΦDC, *in-silico* resulted in a proportional

increase in total cognate effector TCs and initially proportional increase in cognate $CD8^+$ TCs that proceeded towards a plateau (Fig 6D-F). Cognate $CD8^+$ TCs showed a significant response in some simulations, or little response in others (Fig 6D). These results are similar to those following injection of increasing doses of antigenic agent to mice, or agDCs to $CD8^+$ TC culture, showing an initial proportional increase in $CD8^+$ proliferation that gradually reached a plateau (Fig 6A,C) [62]. Total TC response and number of cells of the LNs has also been observed to increase in a linear fashion (Fig 6C) [63].

Fig 6. TC responses *in-silico* and *in-vivo* when the DC stimuli (no. of DCs applied as a fraction of initial TCs present, ϕDC) is varied. The estimated percentage of CD8+ TCs that underwent a proliferative response (A) in the LNs of chimeric mice 7 days post-injection with antigen LM-GP33 and (B) in cell culture post-application of DCs. (C) Similarly, total cell counts of the draining LN, after doses of mature DCs were injected into mice, show an increase in TC numbers that plateaus with increasing dose. (D) Analysis of *in-silico* $CD8^+$ TC response at low doses showed a significant response (1e4 total cognate $CD8^+$TCs) or no proliferative response at all (<10 cognate $CD8^+$TCs). (E) *In-silico* simulations increasing the proportion of DCs resulted in increasing numbers of cognate $CD8^+$ TCs that plateaued as the DC dose increased, a pattern reflected in the overall total number of effector TCs (F).

To replicate murine experiments disrupting agDC presence, simulations were performed eliminating agDCs 12 hours post-entry (instead of permitting a 60 hour lifespan). This resulted in a 91% reduction in peak cognate $CD8^+$ TC peak (S4 FigC). This compares well with results observed when transgenic DT-sensitive agDCs were injected into murine LNs, then eliminated by injecting DT 1 or 12 hours later, which resulted in a 93% and 85% decrease in $CD8^+$ TC magnitude respectively when compared to no-elimination (S4 FigA) [64].

Abrogating $S1P_1r$ down-regulation after antigenic stimulus detection *in-silico*, reduced the number of activated TCs in the paracortex by 60%, 72% and 81% at V_{max}=1.2 ,2.0 and 2.5 (Figure S5D). This was a smaller reduction than observed during *in-vivo* experiments when activated TCs maintaining $S1P_1r$ expression were transferred to LNs, resulting in 90% less activated TC retention in the LNs 15 hours later compared to control mice (S5 FigA) [32]. The *in-silico* reduction was, however, greater than the 40% reduction in activated TCs found with constitutive TC expression of $S1P_1r$ *in-vivo* post-immunisation (S5 FigB) [65]. The *in-silico* total number of $CD4^+$ and $CD8^+$ effector TCs reached 20% and 6% respectively of the control response when $S1P_1r$ was

abrogated (S5 FigE,F). This is similar to the 27% and 5% of control response recorded with constitutive inhibition of $S1P_1r$ expression *in-vivo* (S5 FigC) [65].

Paracortical swelling consistently aids TC activation but not effector TC production

When maximal swelling (V_{max}) was varied from 1 to 2.8, activated TC number positively correlated with V_{max} ($p<10^{-5}$) doubling in number (Fig 7A). However, total number of effector TCs negatively correlated with V_{max} ($p<10^{-4}$) and decreased by 15% (Fig 7B). Neither the number of effector TCs that exited by day 10, nor total number of cognate $CD4^+$ TC present varied significantly (S6 FigB,C). However, total cognate $CD4^+$ TCs that left the paracortex by day 10 increased by 30% and positively correlated with V_{max} (p=0.001) (Fig 7C). $CD8^+$ TC numbers showed the opposite pattern. There was no change in the number of exited cognate $CD8^+$ TCs (S6 Fig.D) but the total number of cognate $CD8^+$ TCs present decreased by 25% and negatively correlated with V_{max} ($p<10^{-4}$) (Fig 7D). The maximum rate of TC recruitment positively correlated with V_{max} and TC egress rate increased with V_{max} from day 6-10 (Fig 7E,F).

Fig 7. The variation in TC subsets as V_{max} was varied from 1 to 2·8 with $T_{mid} = 10^5$. (A) The total activated no. of TCs in the paracortex incrementally increased with V_{max} and doubled in number between V_{max}=1 and 2.8. (B) The total no. of effector TCs decreased 0.3x with increasing V_{max}. (C) The total no. of cognate $CD4^+$ TCs that exited positively correlated with V_{max} (r=0.87, p=0.001) and increased 1.3x. (D) The total cognate $CD8^+$TCs negatively correlated with V_{max} (r=-0.92, p=1.28e-4). (E,F) Peak entry and peak exit rate increased proportionally to V_{Max}. All results are the mean of n¿=7 simulations with SEM displayed. (E) Total TCs in the paracortex.

Analysis of the number of TCs a DC contacted from 30 hours post-infection onwards showed that contact became more significant during simulations permitting a larger swelling, but increased contact did not necessarily result in more activated or effector TCs. At V_{max}=2.0, a positive correlation was observed between effector TCs produced and contacts whereas at V_{max}=1.2, there was no significant correlation (Fig 8A,B). However, as swelling increased, the mean number of cognate TCs a DC contacted decreased ($p<10^{-4}$) (Fig 8C). The number of non-cognate TCs a DC interacted with positively correlated with V_{max} ($p< 10^{-4}$) (S6 FigA). Activated TC numbers negatively

correlated with cognate TC contacts as V_{max} increased (p=0.002) (Fig 8D). Up to V_{max}=1.8, the number of effector TCs present increased with contacts (Fig 8E) but contacts had no effect on the number of exited effector TCs (S6 FigI). The number of cognate TC to DC contacts negatively correlated with cognate $CD4^+$ TCs exited (p= <0.05), positively correlated with total $CD8^+$ TCs ($p< 10^{-5}$), and showed no correlation with cognate $CD4^+$ TCs present or $CD8^+$ TCs exited (Fig 8F,G & S6 FigG,J).

Fig 8. Changes in the number TCs a DC contacts. (A) At V_{max} =1.2, analysis of individual simulations showed a slight linear but non-significant correlation between total effector TCs produced and cognate TCs contacted (r=, 0.52, p= 0.12). (B) At V_{max}=2.0 there was a significant positive linear correlation between cognate TCs contacted by DCs and total effector TCs (p=0.0066). (C) When varying V_{max}, the mean number of cognate TCs contacted by DCs (n=10) negatively correlated with V_{max} r=-0.92, p= 2.02e-04), with a polynomial fit with 2 degrees (R2=0.86) displayed. (D) The mean no. of total activated TCs negatively correlated with TCs contacted, which occurred as V_{max} became larger (2 degree exponential fit, r=-0.85, p=0.002). (E) The mean no. of total effector TCs, positively correlated with TCs contacted, r=0.93 p= 7.6e-05 (linear fit p=4.21e-05). (F) The mean no. of total $CD4^+$ TCs that exited the paracortex negatively correlated with mean TCs contacted by DCs r=0.75, p=0.013, (linear fit p=0.013). (G) The mean no. of total $CD8^+$ TCs in the paracortex positively correlated with TCs contacted, r=0.93, p=7.63e-05, which increased as V_{max} became smaller (linear fit p=7.63e-05).

Varying the ease of swelling influences resulting TC populations.

In some cases, varying the required number of T cells present to reach half the maximal swelling, (T_{mid}), counteracted the effect of varying maximal swelling of LNs on effector TC production. When simulations were carried out with a lower or higher T_{mid} of 8e4 or 12e4, and a small (V_{max}=1.2) or large (V_{max}=2.5) maximal swelling, a similar number of effector TCs were produced with a low T_{mid} and low V_{max} compared to with a high T_{mid} and high V_{max} (Fig 9C). The difference in effector TC response appeared to be due to cognate $CD8^+$ TC behaviour, as there was no significant difference in cognate $CD4^+$ TCs numbers with T_{mid}=8e4 or 12e4 at either V_{max}=1.2 or 2.5 (Fig 9D,E). With a lower T_{mid} of 8e4, paracortex swelling began one day earlier than with T_{mid}=12e4 (Fig 9A). Most TCs were activated with a low T_{mid} and high V_{max}, however at least 40% more activated TCs were recorded when V_{max} was high compared to when V_{max} was low regardless of T_{mid} (Fig 9B). Further simulations varying T_{mid}

with a wider maximal swelling range confirmed that the number of activated TCs increased with expansion, but at every value of V_{max}, correlated negatively with T_{mid} (Fig 10A), which suggests that earlier swelling, whether induced by larger T_{mid} or V_{max}, aids initial TC activation.

Fig 9. Increasing T_{mid} counteracts the loss in effector TCs with V_{max}. (A) The paracortex volume change using different parameter combinations of V_{max} and T_{mid}. (B) Activated TCs increased at larger values of V_{max}. At V_{max}=1.2 there was no significant difference when $T_{mid} = 8^5$ or 10^5 (t-test p=0.12), but a significant difference at V_{max}=2.5 (p=0.002). (C) Increasing T_{mid} at V_{max}=2.5 meant effector TC numbers became the same or more than at V_{max}=1.2. (D) Total $CD4^+$ TCs increased with V_{max} only, and showed no significant difference with T_{mid}=8e4 or 12e4. (E) Total $CD8^+$ TCs exited reflected the pattern of overall effector TCs.

Fig 10. Increasing T_{mid} decreases the number of activated TCs as swelling increases (A) but results in more total effectors TCs (D) and effector $CD8^+$ TCs (E) that leave the paracortex. (B,C). The number of DC and cognate TCs shows no correlation at small swelling values and positive correlation at larger values when T_{mid} is increased. (F) Effector $CD4^+$ TCs that exit show a negative correlation with T_{mid} at smaller swelling values (V_{max}= 1.2 and 1.5) only. G.Repeating the initial simulations but increasing T_{mid} from 10e5 to 12e5 results in the disappearance of the negative effect of swelling on effector TCs exited and (H) Cognate $CD8^+$ TCs exited. (I) Cognate $CD4^+$ TCs continue to increase with swelling. No clear correlation is seen with V_{max} and DC contacts with cognate TCs (J) or activated (K) and effector (L) TCs produced.

Increasing the range of maximal swelling values also showed that the larger V_{max}, the greater the influence of T_{mid} on the number of effector TCs produced. When maximal swelling was smaller ($V_{max} < 1.5$), varying T_{mid} did not significantly affect the total number of effector TCs. However, with larger maximal swelling, increasing T_{mid} from 10^4 to 13^4, thus delaying swelling, resulted in a 20-40% increase in effector TCs (Fig 10D). Production of cognate $CD4^+$ TCs may be aided by a lower T_{mid} and earlier expansion, as at a lower V_{max}, increasing T_{mid} showed a trend towards less cognate $CD4^+$ TCs leaving the paracortex, although this did not reach significance (at V_{max}=1, p=0.08 and at V_{max}=1.5, p=0.051) (Fig 10F). However, at larger swelling no benefit is gained by varying T_{mid} as total cognate $CD4^+$ TC numbers increased with V_{max} regardless of T_{mid} value. Therefore, the increased effector TC number with high T_{mid} and V_{max} is mainly due to $CD8^+$ TCs, with the number of cognate $CD8^+$ TCs that exited paracortex correlating positively with T_{mid} (p=<0.05) at a high V_{max} (Fig 10E).

TC and DC contacts were consistent with the earlier results (Fig 8C) that at a

larger paracortical expansion, with each value of T_{mid}, the overall number of cognate TCs contacted was less than when the same value of T_{mid} was applied with a smaller paracortical expansion (Fig 10B,C). However, at the larger maximal swelling value of 2.5, as T_{mid} increased, the DCs contacted more cognate TCs. At V_{max}= 2, no correlation between contacts and overall cognate TC number occurred (S7 FigA), but a positive correlation was observed between contacts and effector TCs produced ($p<10^{-3}$), $CD8^+$ TCs produced (p=0.03) and $CD8^+$ exited (p=0.027) (Fig 10D,E). At lower values of V_{max}, no similar correlations were observed.

When maximal swelling was varied in 0.2 increments with a higher T_{mid} (12e5), the number of cognate $CD8^+$ TCs no longer decreased with V_{max}, and an intermediate swelling of 1.8-fold became the optimum V_{max} to produce effector TCs. At V_{max}=1.8, 7% more total effector TCs and cognate $CD8^+$ TCs exited than at any other value of V_{max} (Fig 10G). TC activation was also 40% higher than the value at V_{max}=1.0, but less than the 120% increase at V_{max}=2.6 (S7 FigB). In contrast, no correlation was observed between the number of TCs contacted and number of activated TCs produced at different values of V_{max} or the number of cognate TCs contacted and the number of effector TCs exited (Fig 10K,L).

Degree of swelling influences sensitivity of the model to parameter variations.

A parameter sensitivity study revealed that the identified correlations between parameters and measured output (measures of TC activation and differentiation), often reversed or no-longer showed correlation during simulated weeks 1 compared to week 2, and between simulations with fixed volume or expanding LNs. This provides additional evidence that swelling dynamics influence effector TC response. In a fixed paracortical volume a strong positive partial-rank-correlation coefficient was presented by several parameters that would logically drive TC activation and proliferation, such as starting proportion of cognate TCs (F_{cog}) ($p<10^{-6}$) or fraction of DCs (ΦDC) ($p<10^{-6}$), with TC activation and effector TC production (Table 1,2 and S1 Table). However, when paracortical expansion was allowed, a positive correlation was observed in the first week only. The effect of V_{max} also reversed between weeks one and two, positively correlating

to activated TCs in the paracortex up to day 4 and 6 ($p<0.05$) but negatively correlating from day 6 ($p<10^{-6}$) with activated TCs, effector TCs present and effector TCs exited (Table 1 and 2, S1 Table-S3 Table). Another example of a parameter that changed TC dynamics is the duration of DC entry (DC_{in}). Reducing DC_{in} while maintaining the number of entering DCs activates TCs earlier, whereas increasing it facilitates sustained but slower TC activation (Table 1). An additional sensitivity analysis increasing the upper-range of $S1P_1r$ down-regulation on activated TCs (SP_{act}), from 0.4 to 0.8, eliminated the correlation between V_{max} and effector TCs (Table 3). These results suggest that V_{max} can mask the effects of SP_{act} or conversely, maintaining a low SP_{act} value diminishes the effects of V_{max}. Overall, the most influential parameters were those related to $S1P_1r$ regulation of activated TCs, early effector TCs and memory TCs (SP_{act}, SP_{early}, SP_{mem}), signal shape (ΦDC, DC_{in}), frequency of TC cognition (F_{cog}), TC recruitment (Rf, RT2) and paracortical expansion (V_{max} and T_{mid}). Additional results are shown in S1 Table,S2 Table and S3 Table.

Table 1. Parameters that significantly affected number of activated TCs. Present in the paracortex from day 2 to 6 post-stimuli, in a fixed volume and an expanding paracortex.

	With Swelling					Without Swelling				
Parameter	Day2	Day 3	Day 4	Day 5	Day 6	Day 2	Day 3	Day 4	Day 5	Day 6
Max_{NT}						+				
F_{cog}	+++	+++	+++	+++	++	+++	+++	+++	+++	++
DC_{ϕ}	+++	++	+++			+++	+++		++	++
T_{DCin}	−−−	−−−	++	+++	+++	−−−	−−	+	+++	+++
R_F		+++	+++		−		++	++		
V_{Max}	+	+++	+++		−	n/a	n/a	n/a	n/a	n/a

Key : +/-= $0.05> p >0.001$ ++/− =$0.001> p >10^{-6}$ +++/— = $p< 10e^{-6}$

Table 2. Parameters that significantly affected the number of effector TCs that exited the paracortex. From day 3 to 12 post-stimuli. During week 2 post-stimuli, with the expanding model, the value of many parameters correlated negatively with the number of effector TCs that exit the LN, despite some of these parameters showing a consistent significant positive influence or a lack of influence when swelling is not permitted.

Parameter	Day 3	Day 4	Day 5	Day 6	Day 7	Day 8	Day 9	Day 10	Day 11	Day 12
Without Swelling										
TP_{4+}						+	+			
Max_{P8+}					+	+				
γ				−	−−	−−	−	−	−	−
F_{cog}	+++	+++	+++	+++	+++	+++	++	++	++	++
ϕ_{DC}		+								
T_{DCin}		−−−	−−−	−−						
SP_{early}	+++	+++			+	−	−−	−−	−−	−
V_{Max}	n/a	n/a	n/a	n/a	n/a	n/a	n/a	n/a	n/a	n/a
T_{Mid}	n/a	n/a	n/a	n/a	n/a	n/a	n/a	n/a	n/a	n/a
With Swelling										
TP_{4+}										
Max_{P8+}						−−	−−	−−	−	
γ			−	−	−					
MHC_i							−−	−−	−	−
F_{cog}	+++	+++	+++	+++	+					
DC_{ϕ}	+				−−	−−	−−	−−	−−	−−
T_{DCin}	−−−	−−−	−−	−						
SP_{early}	+++									
SP_{mem}					−					
R_F					−−	−−	−−	−−	−−	−−
V_{Max}	−−			−−	−−−	−−−	−−−	−−−		
T_{Mid}	−−									

Key : +/-= 0.05> p >0.001 ++/− =0.001> p >10^{-6} +++/— = p< $10e^{-6}$

Table 3. Parameters that significantly affected the number of activated TCs, in an expanding paracortex from day 2 to 6 post-stimuli, after increasing the upper range of SP_{act}. V_{max} was no longer significantly influential and instead SP_{act} became significantly influential. The parameters involved in TC recruitment RF and RT2, while still important, became less significantly influential.

	With Swelling				
Parameter	Day2	Day 3	Day 4	Day 5	Day 6
Max_{NT}					
F_{cog}	+++	+++	+++	+++	++
DC_{ϕ}	+++		++	++	
T_{DCin}	−−−	−−	+	+++	+++
SP_{act}	−−				
SP_{mem}				−	
RT2		+	+		
R_F		++	+	+	
T_{mid}				−	

Key : +/-= 0.05> p >0.001 ++/− =0.001> p >10^{-6} +++/— = p< $10e^{-6}$

Changes in TC crowding impact effector TC response

The average TC to grid compartment ratio fluctuated within realistic levels in most simulations (0.6-1.3 in a volume equivalent to 1.75 TCs) (Fig 11A). However, when swelling was not permitted, non-physiological average levels above 1.75 and up to 2 occurred, due to rules permitting up to two cells per grid-compartment to prevent gridlock. TCs were modelled as spheres occupying 57% of a grid compartment, therefore a value of 2 exceeds the maximal average physiological ratio of 1.75. Simulations allowing TCs that shared a grid compartment additional opportunities to exit per step resulted in a significant difference in effector TC production at V_{max}= 1.0 and V_{max}= 1.4, but no overall trend was observed (Fig 11B). However, when TCs were permitted to re-enter HEVs with a low probability (P_{e2}), in a fixed-volume paracortex, the TC to grid ratio peaked at 1.6 instead of 2.0, and an average 10% decrease in total number of effector TCs was observed (Fig 11C,D). There remained a positive correlation with activated TCs and V_{max} ($p<10^{-5}$) (S8 Fig), and although the number of effector TCs still decreased, the correlation was less significant and weaker (R=-0.8, $p<10^{-3}$) (Fig 11D).

Fig 11. The effect of varying egress methods and LN maximal swelling. (A) Under original modelling conditions, when swelling was permitted, the TC to grid compartment ratio did not exceed expected levels (1.75) (B) Comparison of effector TC response when increased egress with crowding was applied with no overall trend. (C) When TCs were permitted to return to HEVs with a small probability, less TCs were present in the LN at one time and the ratio of TCs to grid compartments remained within physiological levels (<1.75), even in a fixed volume LN. Slightly less effector TCs were produced at all values of V_{max} but this was only significant at V_{max}= 2.2 and 2.8 *=t-test $p<0.05$.

$S1P_1$r-mediated temporary retention of early effector TCs increased TC response

Regardless of permitted maximal swelling, down-regulating $S1P_1$r on early effector TC to less than 80% of naïve TC expression (SP_{Early} <0.8) produced a sustained increase in total TCs, despite the action only directly affecting the small subset of early effector TCs (Fig 12A). Reducing SP_{early} to 0.4 doubled the total number of effectors TCs, whilst SP_{early} =<0.1 increased the number of effector TCs that left the node by day 10 by 3-fold (Fig 12G). The number of effector TCs that exited continued to increase as

SP_{early} was reduced to 0.05 with larger paracortical swelling only (V_{max} >=2). The most effector TCs were produced at the smallest value of SP_{early} and largest maximal swelling (Fig 12G). When analysing the TC sub-populations, the number of both $CD4^+$ and $CD8^+$ effector TCs that exited the paracortex by day 10 increased 3-4 fold with $SP_{early} < 0.1$ (Fig 12H,I). No further increase in $CD8^+$TCs exited was observed when SP_{early} was decreased to 0.05.

Fig 12. Varying SP_{early} and thus retention of newly differentiated TCs. (A) Reducing SP_{early} resulted in a higher total number of TCs in the paracortex. (B) At V_{max}=1.2, reducing SP_{early} to <0.1, despite retaining TCs, increased peak TC egress rate above the peak rate at baseline SP_{early}. D.At V_{max}=2.5, reducing SP_{early} did not result in TC egress exceeding the peak rate at baseline SP_{early}. (C,E) At V_{max}=1.2 and 2.5, the TC-to-grid ratio was increased in the second half of the simulation when SP_{early} was reduced. (E) At the larger V_{max}=2.5, SP_{early}<0.4 maintained the peak TC-to-grid ratio for 4 days. (F) The number of activated TCs increased with V_{max} and was unaffected by SP_{early}. (G) Effector TCs that exited the paracortex were influenced more by SP_{early} than by V_{max}. The most effector TCs exited when SP_{early} was <=0.1 and when V_{max}=2. (H) The highest number of $CD4^+$ TCs exited when SP_{early} was at the smallest value and V_{max} at the largest value. (I) The highest number of $CD8^+$ TCs exited when SP_{early} was smallest (0.05) and maximal swelling intermediate (V_{max} =2.0). (J) The mean number of cognate TCs contacted decreased with more paracortical swelling (>V_{max}) but increased as SP_{early} decreased to 0.1.

To explore the accompanying effects of $S1P_1$r-mediated increase in effector TC production, we analysed the accompanying alterations in TC and DC interaction, the proportion of TCs to paracortical volume and the TC exit rates. At all values of V_{max}, there was a 3-fold increase in the mean number of TCs contacted by DCs when SP_{early} was decreased from 0.8 to 0.1 (Fig 12J). However, when SP_{early} was >=0.1, at larger values of V_{max}(>=2.0), despite less DCs and cognate TCs contact, the same number or more effectors TCs exited than at smaller swellings. Other changes with a lowered SP_{early} of <=1 included an increase in TC egress rate that was sustained for two days longer, and at V_{max} <2.0, a doubling of TC egress rate from days 1-5, compared to simulations with V_{max} =>2 (Fig 12B,D). By day 6 to 8, TC egress rate was similar between values of V_{max}. Despite increase in TC egress the TC to grid-compartment ratio also increased with SP_{early} <=0.1 therefore TC egress did not exceed TC production (Fig 12.C,E). However, the TC to grid-compartment ratio was highest at lower values of V_{max} and SP_{early} <0.1, but this parameter combination did not produce the most effector TCs, suggesting the balance between retention and increase is key for efficient TC production.

Discussion

In this work we aimed to better understand the role of lymph node swelling and other adaptive immune processes in the formation of TC responses. Our study builds on methods used in previous work that confirmed the ability of ABMs to predict immune cell behaviours [37, 39–41, 43]. Model validation was accomplished by comparing predictions to a range of published experiments, and robustness was confirmed by multiple parameter variation analyses. By varying paracortical swelling and $S1P_1r$ expression, we showed that paracortical swelling aids TC activation, but early swelling can impair effector TC response. However, temporary retention of newly differentiated TCs influences the overall effector TC response more than swelling, providing a mechanism to overcome swelling-induced impairment.

A key finding from our study was the strong influence of $S1P_1r$ down-regulation on newly differentiated effector TCs on the number of effector TCs produced during immune response (Fig 12). Our study focused on the effect of temporary down-regulation of $S1P_1r$ on effector TCs that can amplify overall response, whereas previous studies have focused on the inhibitory effects of permanent $S1P_1r$ down-regulation. Induction and maintenance of $S1P_1r$ down-regulation on all TCs present is the mechanism of the recently developed multiple sclerosis drug Fingolipid, to prevent effector TCs migrating to the brain and participating in autoimmune response [77]. Inhibition of $S1P_1r$ expression on effector TCs only has also been carried out *in-vivo* [24]. However, temporary down-regulation on selectively newly differentiated TCs may prove technically difficult, suggesting identification of alternative means of retention is desirable.

Another key finding was that the initial 5 days of paracortical swelling facilitates the retention of activated TCs in the LNs (Fig 7A). Both TC recruitment and TC egress increase with swelling (Fig 7E,F) and therefore overall TC trafficking rate is increased, yet activated TCs are retained due to $S1P_1r$ down-regulation. When $S1P_1r$-mediated retention is removed, depleted activation is observed *in-silico* and *in-vivo* (S5 Fig) and our simulations show that swelling no longer aids activation. Additionally, increased TC recruitment with HEV growth that accompanies swelling allows more cognate TCs to enter, an effect that is amplified when activated TCs proliferate. TC activation did not

appear to be constrained by DC and TC interaction during these simulations, as the mean number of cognate TCs a DC interacted with decreased with swelling, despite the increased space for TC migration and access (Fig 8C).

Thirdly, our results suggest that swelling of LNs too early can negatively impact TC response, by reducing the total number of effector TCs and the number of exiting effector $CD8^+$ TCs (Fig 10). Conversely, delaying swelling (increasing T_{mid}) can result in just as many, if not more effector TC exiting the paracortex by day 10, as long as sufficient swelling is permitted (>1.5-fold). Delayed swelling allows for TC recruitment and retention to be a stronger influence than TC egress in the initial few days, possibly by reducing access to the number of exit points, as increased swelling increases TC egress rate. The multi-phase nature of these responses is supported by the results of the global sensitivity analysis, which showed that the influences of several parameters switched over time in the presence of node swelling (Table 1-3).

We also observed that early swelling hindered the $CD8^+$ effector TC response more than $CD4^+$ TCs, potentially due to the later and longer duration of simulated $CD8^+$ TC proliferation [78]. Earlier proliferation of $CD4^+$ TCs in the model may mean that a point of exponential proliferation is reached such that further proliferation is proportionally less affected by increases in TC egress that accompany paracortical swelling than $CD8^+$ TCs. Space to move and contact DCs may also limit CD8+ TC proliferation. Analysis of DC and cognate TC contacts suggested that increased contact only became more influential at larger paracortical swelling only (Fig 8A,B). As $CD8^+$ TCs undergo more proliferation at the later stages in the response, with increased space and less remaining stimulus, each individual TC-DC interaction becomes more important.

The insight provided by our results imply that limiting effector TC production could be achieved by facilitating early swelling of LNs, or an immune dysfunction in chronically inflamed LNs, could be addressed by modulating swelling. Physiologically, factors that could be manipulated to alter the effective T_{mid} include stromal cell contractile behaviour and proliferation rate, the sensitivity of immune response to antigen signalling, and the sensitivity to accumulated fluid and TCs. Astarita et al. [2015] induced swelling by transferring 10^6 cognate TCs directly into murine LNs, whilst also effectively modulating T_{mid} by inducing FRC elongation and inhibiting FRC

contraction. Subsequent TC proliferative response was enhanced by the facilitated swelling. However, as both *in-silico* and *in-vivo* experiments have shown, proliferative response size is proportional to the starting frequency of cognate TCs [21, 59, 61] (S3 Fig). Therefore, with an inflated number of initial cognate TCs, the time-point at which swelling of LNs becomes helpful is likely shifted forward. Furthermore, the differential response of $CD4^+$ and $CD8^+$ TCs suggests modulating swelling of LNs could influence differential downstream immune response pathways. However, this differential behaviour is partly due to the assumption of earlier $CD4^+$ 'Helper' TC activation behaviour. The model could be used to further investigate scenarios whereby timing of $CD4^+$ and $CD8^+$ response may vary with different stimuli, by varying activation and differentiation parameters,

Validation of the model was achieved by replicating a range of published studies. Some slight differences were observed, for example, the effect of *in-silico* elimination of agDCs after 12 hours more closely matched *in-vivo* elimination of DCs after 1 hour rather than 12 hours. This is possibly because *in-vivo*, although most DCs were removed within 6 hours post-DT injection, 12 hours were required to eliminate virtually all DCs. Additionally, *in-silico* prevention of $S1P_1r$ down-regulation on activated TCs resulted in a smaller reduction in activated TC number (60-80%) than the 90% described by Lo *et al* 2004, but more than the 40% reported by Gräler *et al* 1997. However, this discrepancy may be because the 40% figure was recorded after accounting for reduced naive TCs homing to the LN due to the lack of $S1P_1r$ expression, prior to possible TC activation that was subsequently also affected.

A limitation of the model is that paracortical expansion is dependent only on TC numbers, but physiologically this is due to other factors that are not explicitly included, such as stromal cell proliferation rate. It would be a minor adaptation to the model to represent explicitly the effects of both innate and adaptive signalling pathways that regulate such factors. The use of a sigmoidal function to dictate paracortical volume allows an initial increase in TCs without triggering significant swelling. This reflects an initial inhibition of stromal cell proliferation by increased secretion of IFN type 1 [79]. The delayed increase in volume in response to TC number then reflects the switch in signalling at day 2 to favour LEC proliferation and expansion of LNs, through mechanisms such as DC-induced secretion of VEGF from stromal cells and increased

elasticity of FRC network [9, 80]. Furthermore, TC numbers are impacted by retention, but the effects of regulation of TC expression of chemokine-receptor CCR7 and the role of chemo-attraction in locating and retaining TCs in the paracortex was omitted [50]. When both CCR7 and $S1P_1r$ expression on TCs was inhibited *in-vivo*, the TCs migrated to the edges of the paracortex, due to the loss of chemo-attraction deep within the paracortex, but could not exit due to lack of $S1P_1r$ expression. Accordingly, inclusion of $S1P_1r$ down-regulation was prioritised over CCR7 but the identified strong influence of retention suggests future models should include a wider range of retentive influences [24].

In future iterations of the model, inclusion of additional factors such as lymph flow and pressure alterations (along with fluid exchange with nodal blood vessels), could also significantly improve the representation of swelling, and thus TC egress and retention. It has long been known that changes in hydrostatic and oncotic pressure differences across nodal blood vessel walls can reverse the net fluid exchange [81, 82]. Afferent lymphatic flow to the LNs also increases with immune response. Therefore, a key next step is to couple the ABM to a computational flow models while resident DCs in the LNs could also be added and the maximal permitted swelling increased to confirm the observed trends.

Conclusion

Our results here suggest that although swelling of LNs may aid TC activation, avoidance of excessive swelling of LNs may boost effector TC response when initial TC response is small, for example, in immuno-suppressed patients or when optimizing vaccine design to minimise antigen dose. Moreover, retention of newly differentiated TCs via the modulation of the TC receptor Sphingosine-1-phosphate-1-receptor ($S1P_1r$) showed that selective modulation on the small subset of effector TCs could strongly impact the efficiency of the TCs response and overcome loss in efficiency of TC response due to early enlargement. Although permanent blockade of effector TC egress has been utilised to treat multiple sclerosis, temporary retention of effector TCs to boost subsequent effector TC production presents as a novel mechanism. This finding also emphasizes the influence that retentive features, including factors such as chemokines, may have on

effector TC response, that may be more practical *in-vivo* targets to manipulate.

Supporting information

S1 File. Supplementary Methods S1.1 T cell recruitment. S1.2 Agents and agent migration. S1.2 Agent interaction and signal integration.

S2 File. Parameter File Tables of parameter values and sources.

S3 File. UML diagrams description.

S1 Fig. A class diagram displaying the underlying ABM structure. The model is constructed using instructions in the 'context builder' class. The entire modelling domain is described by the context class, and each compartment of the domain is described by the GridCell class. In a 3D simulation, each grid cell can be queried to identify the 26 neighbouring grids and how many agents they contain. The TC class is a template for the T cell object produced and is instantiated thousands of times to create T cells with the same variables but slightly different values. A subclass of cognate T cells extends the template to contains more methods and variables relating to interaction and proliferative response

S2 Fig. Captured phases of TC trafficking and response to AgDC stimuli. Changes in proliferation and differentiation continued after the initial stimulus was no longer present. TC recruitment and TC egress changes also accompanied the response.

S3 Fig. TC responses *in-silico* and *in-vivo* when proportion of cognate TCs was varied. A. $CD4^+$ magnitude of response in dLNs of mice to injected antigen correlated to starting estimated frequency of cognate TCs in a sample of $1x10^7$TCs). B. Results in-silico showed an overall increase in response with increasing F_{cog} (n=8). Simulations using a wider range of F_{cog} values (C,D) confirmed no. of total cognate $CD4^+$ TCs and $CD8^+$ TCs increased linearly with F_{cog}. E. Mice were infected with VSV-M45 or VSV-ova with starting precursor $CD8^+$ frequencies of 7e-5,8e-5 and 13e-5 respectively. The peak number of resulting TCs as a percent of overall $CD8^+$ TCs

present is shown.F. Simulations using the same F_{cog} *in-silico* showed a similar increasing trend with similar increase rate.

S4 Fig. TC responses in-silico and in-vivo when a stimulus is abruptly abolished. A. Transgenic Rats were used that would eliminate specific injected agDCs when the rat was injected with DT within 12 hours. The rats were injected with OT-1 $CD8^+$ TCs specific for agDCs that were subsequently injected. DT was then injected at 1h,12 and 48hr(not-shown) later, curtailing the time that the agDCs would normally spend in the LN. Adapted from Prlic et al 2006. B. The simulated disrupted input stimuli achieved by curtailing the 60hr DC influx at 12+-2hr. C-D. The results of simulations (n=8). Mean (+-SEM) $CD8^+$ TCs were reduced 91% when the stimulus was curtailed at 12hrs compared to sustained entry for 60hrs. D. individual CD8+ TC responses varied by a factor of 10 in an all or nothing response manner.

S5 Fig. TC responses in-silico and in-vivo when $S1P_1r$ down-regulation is inhibited. A. Pre-activated wildtype TCs ($S1P_1r$) and pre-activated TCs over-expressing $S1P_1r$ ($S1P_1r$++) were transferred into mice and further entry of TCs was blocked. 15hrs later there was a 90% reduction in retention of $S1P_1r$++ activated TCs. Adapted from Lo et al 2005. B. The number of activated TCs in the LNs 24hours post-transfer dropped by 40% in transgenic mice with constitutive $S1P_1r$ expression while (C) the proliferative $CD4^+$ and $CD8^+$ TC response decreased to 20% and 6% of that of the wild- type mice. Adapted from Gräler et al 1997. D-F. Simulation results (n=10) where $S1P_1r$ down-regulation was prevented (-SP regulation), compared to baseline simulations (+SP regulation). Mean (+-SEM) total number of activated TCs present was reduced 60%, 72% and 81% at V_{max}=1.2,1.5 and 2. E. The mean (+-SEM) number of total $CD8^+$ TCs, was diminished to 25,15 and 18% of control response at V_{Max}=1.2,1.5 and 2.0. F. $CD4^+$ TCs were similarly diminished to 8-10% of control at all values of V_{max}.

S6 Fig. Additional data when V_{Max} was varied with T_{mid}=10e4 TCs. A. The number of non-cognate TCs a DC contacted increased with LN swelling. B. No significant difference was apparent when effector TCs exited were plotted over time. C. Total cognate $CD4^+$ TCs in the paracortex. D. Total $CD8^+$ TCs that exited the

paracortex. E,F. The total TCs present in the paracortex over the course of the simulation decreased as V_{max} increased, up to V_{max}=2.0 at which no further difference was observed (H). G, I, J. No correlation was observed between swelling, TC and DC contact and total cognate $CD4^+$ TCs or Effector/cognate $CD8^+$ TCs that exited by day 10.

S7 Fig. Cognate TC and DC contact and T cell activation while varying T_{mid} and permitting a larger swelling A. At V_{max}=2.0, no correlation between cognate TC and DC contacts and T_{mid} was observed. B. With a higher T_{mid} of 12e5, there remained a correlation between activated TCs and V_{Max}.

S8 Fig. The activation of TCs at different maximal swelling when allowing TCs to return to HECs with a low probability increases with V_{max}. ($p<10^{-5}$).

S1 Table. Parameters that significantly influenced the number of effector TVs in the paracortex from day 3 to day 12 post-stimuli. There is a greater correlation between maximum $CD8^+$ TC proliferation and effector TCs produced in the expanding paracortex than in the fixed volume paracortex. In an expanding paracortex there is also a negative correlation with TC recruitment, and maximal paracortical swelling in the second week of the simulation.

S2 Table. Parameters that significantly affected memory TCs number in the paracortex. Data is only shown from day 5 to day 12 post-stimuli, as they are not produced in the first few days. At day 5, V_{max} still showed some positive correlation with memory TCs present but by day 7 shows a negative correlation.

S3 Table. Parameters that significantly affected the number of memory TCs exited in the paracortex from day 5 to day 12 post-stimuli.

Acknowledgements

The authors gratefully acknowledge the help and unpublished data provided by Dr Samira Jamalian and assistance of Willy Bonneuil.

References

1. Chang JE, Turley SJ. Stromal infrastructure of the lymph node and coordination of immunity. Trends in Immunology. 2014;36(1):30–39.

2. Mueller SN, Germain RN. Stromal cell contributions to the homeostasis and functionality of the immune system. Nature Reviews Immunology. 2009;9:618–29.

3. Chyou S, Benahmed F, Chen J, Kumar V, Tian S, Lipp M, et al. Coordinated regulation of lymph node vascular-stromal growth first by CD11c+ cells and then by T and B cells. Journal of immunology. 2011;187(11):5558–67. doi:10.4049/jimmunol.1101724.

4. Kumar V, Scandella E, Danuser R, Onder L, Nitschké M, Fukui Y, et al. Global lymphoid tissue remodeling during a viral infection is orchestrated by a B cell–lymphotoxin-dependent pathway. Blood. 2010;115(23):4725–4733. doi:10.1182/blood-2009-10-250118.

5. Yang CYY, Vogt TK, Favre S, Scarpellino L, Huang HYY, Tacchini-Cottier F, et al. Trapping of naive lymphocytes triggers rapid growth and remodeling of the fibroblast network in reactive murine lymph nodes. PNAS. 2014;111(1):E109–18. doi:10.1073/pnas.1312585111.

6. Hay JB, Hobbs BB. The flow of blood to lymph nodes and its relation to lymphocyte traffic and the immune response. Journal of Experimental Medicine. 1977;145(1):31–44.

7. Soderberg KA, Payne GW, Sato A, Medzhitov R, Segal SS, Iwasaki A. Innate control of adaptive immunity via remodeling of lymph node feed arteriole. Proceedings of the National Academy of Sciences of the United States of America. 2005;102(45):16315–16320. doi:10.1073/pnas.0506190102.

8. Cahill R, Frost H, Trnka Z. The effects of antigen on the migration of recirculating lymphocytes through single lymph nodes. J Exp Med. 1976;143(4):870–888. doi:10.1084/jem.143.4.870.

9. Acton SE, Farrugia AJ, Astarita JL, Mourao-Sa D, Jenkins RP, Nye E, et al. Dendritic cells control fibroblastic reticular network tension and lymph node expansion. Nature. 2014;514(7523):498–502.

10. Drayson MT, Smith ME. The sequence of changes in blood flow and lymphocyte influx to stimulated rat lymph nodes. Immunology. 1981;44:125–133.

11. Astarita JL, Cremasco V, Fu J, Darnell MC, Peck JR, Nieves-Bonilla JM, et al. The CLEC-2-podoplanin axis controls fibroblastic reticular cell contractility and lymph node microarchitecture. Nature Imm. 2015;16(1):75–84.

12. Gregory JL, Walter A, Alexandre YO, Hor JL, Liu R, Ma JZ, et al. Infection Programs Sustained Lymphoid Stromal Cell Responses and Shapes Lymph Node Remodeling upon Secondary Challenge. Cell Reports. 2017;18(2):406 – 418. doi:https://doi.org/10.1016/j.celrep.2016.12.038.

13. Kumar V, Chyou S, Stein J, Lu T. Optical projection tomography reveals dynamics of HEV growth after immunization with protein plus CFA and features shared with HEVs in acute. Frontiers in immunology. 2012;7(3):282.

14. Webster B, Ekland EH, Agle LM, Chyou S, Ruggieri R, Lu TT. Regulation of lymph node vascular growth by dendritic cells. J Exp Med. 2006;203(8):1903–13. doi:10.1084/jem.20052272.

15. Tzeng TC, Chyou S, Tian S, Webster B, Carpenter AC, Guaiquil VH, et al. CD11chi Dendritic Cells Regulate the Re-establishment of Vascular Quiescence and Stabilization after Immune Stimulation of Lymph Nodes. The Journal of Immunology. 2010;184(8):4247–4257. doi:10.4049/jimmunol.0902914.

16. Tan KW, Yeo KP, Wong FHS, Lim HY, Khoo KL, Abastado JP, et al. Expansion of Cortical and Medullary Sinuses Restrains Lymph Node Hypertrophy during Prolonged Inflammation. The Journal of Immunology. 2012;188(8):4065–4080. doi:10.4049/jimmunol.1101854.

17. Cyster JG. Chemokines, sphingosine-1-phosphate, and cell migration in secondary lymphoid organs. Annu Rev Immunol. 2005;23:127–59. doi:10.1146/annurev.immunol.23.021704.115628.

18. Braun A, Worbs T, Moschovakis G, Halle S, Hoffmann K, Bölter J, et al. Afferent lymph-derived T cells and DCs use different chemokine receptor CCR7-dependent routes for entry into the lymph node and intranodal migration. Nat Immunol. 2011;12(9):879–87. doi:10.1038/ni.2085.

19. von Andrian UH, Mempel TR. Homing and cellular traffic in lymph nodes. Nature reviews Immunology. 2003;3(11):867–78. doi:10.1038/nri1222.

20. Blattman JN, Antia R, Sourdive DJ, Wang X, Kaech SM, Murali-Krishna K, et al. Estimating the Precursor Frequency of Naive Antigen-specific CD8 T Cells. The Journal of Experimental Medicine. 2002;195(5):657–664.

21. Jenkins MK, Moon JJ. The role of naïve T cell precursor frequency and recruitment in dictating immune response magnitude. Journal of Immunology (Baltimore, Md : 1950). 2012;188(9):4135–4140.

22. Bousso P. T-cell activation by dendritic cells in the lymph node: lessons from the movies. Nature Reviews Immunology. 2008;8:675–84.

23. Pennock ND, White JT, Cross EW, Cheney EE, Tamburini BA, Kedl RM. T cell responses: naïve to memory and everything in between. Advances in Physiology Education. 2013;37(4):273–283.

24. Benechet AP, Menon M, Xu D, Samji T, Maher L, Murooka TT, et al. T cell-intrinsic S1PR1 regulates endogenous effector T-cell egress dynamics from lymph nodes during infection. PNAS. 2016;113(8):2182–2187. doi:10.1073/pnas.1516485113.

25. Youngblood B, Hale JS, Kissick HT, Ahn E, Xu X, Wieland A, et al. Effector CD8 T cells dedifferentiate into long-lived memory cells. Nature. 2017;552(7685):404–9.

26. Wherry EJ, Ahmed R. Memory CD8 T-Cell Differentiation during Viral Infection. Journal of Virology. 2004;78(11):5535–5545. doi:10.1128/JVI.78.11.5535-5545.2004.

27. van Stipdonk MJB, Lemmens EE, Schoenberger SP. Naïve CTLs require a single brief period of antigenic stimulation for clonal expansion and differentiation. Nature Immunology. 2001;2:423–9.

28. Bevan MJ. Helping the CD8+ T-cell response. Nature Reviews Immunology. 2004;4:595–602.

29. Schrum AG, Palmer E, Turka LA. Distinct temporal programming of naive CD4(+) T cells for cell division versus TCR-dependent death susceptibility by antigen-presenting macrophages. European journal of immunology. 2005;35(2):449–459.

30. Parijs LV, Abbas AK. Homeostasis and Self-Tolerance in the Immune System: Turning Lymphocytes off. Science. 1998;280(5361):243–248. doi:10.1126/science.280.5361.243.

31. Matloubian M, Lo C, Cinamon G, Lesneski M, Xu Y. Lymphocyte egress from thymus and peripheral lymphoid organs is dependent on S1P receptor 1. Nature. 2004;427(6972):355–60. doi:10.1038/nature02284.

32. Lo C, Xu Y, Proia R, Cyster J. Cyclical modulation of sphingosine-1-phosphate receptor 1 surface expression during lymphocyte recirculation and relationship to lymphoid organ transit. Journal of Experimental Medicine. 2005;2(201):291–301. doi:10.1084/jem.20041509.

33. Cyster J, Schwab S. Sphingosine-1-phosphate and lymphocyte egress from lymphoid organs. Annual review of immunology. 2012;30:69–94. doi:10.1146/annurev-immunol-020711-075011.

34. Grigorova I, Schwab S, Phan T, Pham T. Cortical sinus probing, S1P1-dependent entry and flow-based capture of egressing T cells. Nature Imm. 2009;10:58–65. doi:10.1038/ni.1682.

35. Hunter M, Teijeira A, Halin C. T cell trafficking through lymphatic vessels. Frontiers in Immunology. 2016;7:613.

36. Bogle G, Dunbar PR. Simulating T-cell motility in the lymph node paracortex with a packed lattice geometry. Imm Cell Biol. 2008;86(8):676–687.

37. Bogle G, Dunbar PR. Agent-based simulation of T-cell activation and proliferation within a lymph node. Imm Cell Biol. 2009;88(2):172–179.

38. Bogle G, Dunbar PR. On-lattice simulation of T cell motility, chemotaxis, and trafficking in the lymph node paracortex. PloS one. 2012;7(9):e45258.

39. Brown LV, Gaffney EA, Wagg J, Coles MC. An in silico model of cytotoxic T-lymphocyte activation in the lymph node following short peptide vaccination. Journal of the Royal Society, Interface. 2018;15(140):2018.0041.

40. Celli S, Day M, Müller AJ, Molina-Paris C, Lythe G, Bousso P. How many dendritic cells are required to initiate a T-cell response? Blood. 2012;120(19):3945–3948. doi:10.1182/blood-2012-01-408260.

41. Gong C, Mattila JT, Miller M, Flynn JL, Linderman JJ, Kirschner D. Predicting lymph node output efficiency using systems biology. Journal of Theoretical Biology. 2013;335:169 – 184.

42. Gong C, Linderman J, Kirschner D. Harnessing the Heterogeneity of T Cell Differentiation Fate to Fine-Tune Generation of Effector and Memory T Cells. Frontiers in Immunology. 2014;5:57. doi:10.3389/fimmu.2014.00057.

43. Ziraldo C, Gong C, Kirschner DE, Linderman JJ. Strategic Priming with Multiple Antigens can Yield Memory Cell Phenotypes Optimized for Infection with Mycobacterium tuberculosis: A Computational Study. Frontiers in Microbiology. 2015;6. doi:10.3389/fmicb.2015.01477.

44. Baldazzi V, Paci P, Bernaschi M, Castiglione F. Modeling lymphocyte homing and encounters in lymph nodes. BMC Bioinformatics. 2009;10:387. doi:10.1186/1471-2105-10-387.

45. Jafarnejad M, Woodruff MC, Zawieja DC, Carroll MC, Moore J. Modeling Lymph Flow and Fluid Exchange with Blood Vessels in Lymph Nodes. Lymphat Res Biol. 2015;13(4):234–247. doi:10.1089/lrb.2015.0028.

46. Jafarnejad M, Zawieja DC, Brook BS, Nibbs RJB, Moore JE. A Novel Computational Model Predicts Key Regulators of Chemokine Gradient

Formation in Lymph Nodes and Site-Specific Roles for CCL19 and ACKR4. The Journal of Immunology. 2017;199(7):2291–2304. doi:10.4049/jimmunol.1700377.

47. Kuka M, Iannacone M. The role of lymph node sinus macrophages in host defense. Annals of the New York Academy of Sciences. 2014;1319(1):38–46. doi:10.1111/nyas.12387.

48. Girard JP, Moussion C, Förster R. HEVs, lymphatics and homeostatic immune cell trafficking in lymph nodes. Nat Rev Immunol. 2012;12(11):762–73. doi:10.1038/nri3298.

49. Shiow L, Rosen D, Brdiková N, Xu Y, An J. CD69 acts downstream of interferon-I/I2 to inhibit S1P1 and lymphocyte egress from lymphoid organs. Nature. 2006;440(7083):540–4. doi:10.1038/nature04606.

50. Pham T, Okada T, Matloubian M, Lo C, Cyster J. S1P 1 receptor signaling overrides retention mediated by Gi-coupled receptors to promote T cell egress. Immunity. 2008;28(1):122–133.

51. Garris CS, Blaho VA, Hla T, Han MH. Sphingosine-1-phosphate receptor 1 signalling in T cells: trafficking and beyond. Immunology. 2014;142(3):347–353.

52. Cella M, Salio M, Sakakibara Y, Langen H, Julkunen I, Lanzavecchia A. Maturation, Activation, and Protection of Dendritic Cells Induced by Double-stranded RNA. The Journal of Experimental Medicine. 1999;189(5):821–829.

53. Kukutsch NA, Rossner S, Austyn JM, Schuler G, Lutz MB. Formation and Kinetics of MHC Class I-Ovalbumin Peptide Complexes on Immature and Mature Murine Dendritic Cells. Journal of Investigative Dermatology. 2000;115(3):449 – 453. doi:https://doi.org/10.1046/j.1523-1747.2000.00084.x.

54. Cella M, Engering A, Pinet V, Pieters J, Lanzavecchia A. Inflammatory stimuli induce accumulation of MHC class II complexes on dendritic cells. Nature. 1997;388:782–7.

55. Baumgartner C, Ferrante A, Nagaoka M, Gorski J, Malherbe LP. Peptide-MHC Class II Complex Stability Governs CD4 T Cell Clonal Selection. Journal of immunology (Baltimore, Md : 1950). 2010;184(2):573–581.

56. Latif R, de Rosbo NK, Amarant T, Rappuoli R, Sappler G, Ben-Nun A. Reversal of the CD4(+)/CD8(+) T-Cell Ratio in Lymph Node Cells upon In Vitro Mitogenic Stimulation by Highly Purified, Water-Soluble S3-S4 Dimer of Pertussis Toxin. Infection and Immunity. 2001;69(5):3073–3081. doi:10.1128/IAI.69.5.3073-3081.2001.

57. Linderman JJ, Riggs T, Pande M, Miller M, Marino S, Kirschner DE. Characterizing the Dynamics of CD4+ T Cell Priming within a Lymph Node. The Journal of Immunology. 2010;184(6):2873–2885. doi:10.4049/jimmunol.0903117.

58. Smith CM, Wilson NS, Waithman J, Villadangos JA, Carbone FR, Heath WR, et al. Cognate CD4+ T cell licensing of dendritic cells in CD8+ T cell immunity. Nature Immunology. 2004;5:1143–8.

59. Obar JJ, Khanna KM, Lefrançois L. Endogenous naive CD8+ T cell precursor frequency regulates primary and memory responses to infection. Immunity. 2008;28(6):859–869. doi:10.1016/j.immuni.2008.04.010.

60. Marino S, Hogue IB, Ray CJ, Kirschner DE. A methodology for performing global uncertainty and sensitivity analysis in systems biology. Journal of Theoretical Biology. 2008;254(1):178 – 196. doi:https://doi.org/10.1016/j.jtbi.2008.04.011.

61. Moon JJ, Chu HH, Pepper M, McSorley SJ, Jameson SC, Kedl RM, et al. Naive CD4(+) T cell frequency varies for different epitopes and predicts repertoire diversity and response magnitude. Immunity. 2007;27(2):203–213.

62. Kaech SM, Ahmed R. Memory CD8+ T cell differentiation: initial antigen encounter triggers a developmental program in naïve cells. Nature Immunology. 2001;2:415–22.

63. Martín-Fontecha A, Sebastiani S, Höpken UE, Uguccioni M, Lipp M, Lanzavecchia A, et al. Regulation of Dendritic Cell Migration to the Draining Lymph Node. Journal of Experimental Medicine. 2003;198(4):615–621. doi:10.1084/jem.20030448.

64. Prlic M, Hernandez-Hoyos G, Bevan MJ. Duration of the initial TCR stimulus controls the magnitude but not functionality of the CD8+ T cell response. Journal of Experimental Medicine. 2006;203(9):2135–2143. doi:10.1084/jem.20060928.

65. Gräler MH, Huang MC, Watson S, Goetzl EJ. Immunological Effects of Transgenic Constitutive Expression of the Type 1 Sphingosine 1-Phosphate Receptor by Mouse Lymphocytes. The Journal of Immunology. 2005;174(4):1997–2003. doi:10.4049/jimmunol.174.4.1997.

66. Park E, Peixoto A, Imai Y, Goodarzi A, Cheng G. Distinct roles for LFA-1 affinity regulation during T-cell adhesion, diapedesis, and interstitial migration in lymph nodes. Blood. 2010;115(8):1572–81.

67. Boscacci R, Pfeiffer F, Gollmer K, Sevilla A. Comprehensive analysis of lymph node stroma-expressed Ig superfamily members reveals redundant and nonredundant roles for ICAM-1, ICAM-2, and VCAM-1 in lymphocyte homing. Blood. 2010;116(6):915–25.

68. Park C, Hwang I, Sinha R, Kamenyeva O. Lymph node B lymphocyte trafficking is constrained by anatomy and highly dependent upon chemo-attractant desensitization. Blood. 2012;119(4):978–989.

69. Miller MJ, Wei SH, Parker I, Cahalan MD. Two-photon imaging of lymphocyte motility and antigen response in intact lymph node. Science. 2002;296(5574):1869–73. doi:10.1126/science.1070051.

70. Beltman JB, Marée AFM, Lynch JN, Miller MJ, de Boer RJ. Lymph node topology dictates T cell migration behavior. Journal of Experimental Medicine. 2007;204(4):771–780. doi:10.1084/jem.20061278.

71. Tomura M, Yoshida N, Tanaka J. Monitoring cellular movement in vivo with photoconvertible fluorescence protein 'Kaede' transgenic mice. PNAS. 2008;105(31):10871–6. doi:10.1073/pnas.0802278105.

72. Tedla N, Wang H, HP M. Regulation of T lymphocyte trafficking into lymph nodes during an immune response by the chemokines macrophage inflammatory protein (MIP)-1 and MIP-1I2. The Journal of Imm. 1998;161(10):5663–72.

73. Hugues S, Fetler L, Bonifaz L, Helft J, Amblard F, Amigorena S. Distinct T cell dynamics in lymph nodes during the induction of tolerance and immunity. Nature Immunology. 2004;5:1235–42.

74. Kinjyo I, Qin J, Tan SY, Wellard CJ, Mrass P, Ritchie W, et al. Real-time tracking of cell cycle progression during CD8+ effector and memory T-cell differentiation. Nature Communications. 2015;6:6301.

75. Homann D, Teyton L, Oldstone MBA. Differential regulation of antiviral T-cell immunity results in stable CD8+ but declining CD4+ T-cell memory. Nature Medicine. 2001;7(8):913–919.

76. Hall J, Morris B. The immediate effect of antigens on the cell output of a lymph node. British journal of experimental pathology. 1965;46(4):450–454.

77. Chun J, Hartung HP. Mechanism of action of oral fingolimod (FTY720) in multiple sclerosis. Clinical neuropharmacology. 2010;33(2):91–101.

78. Foulds KE, Zenewicz LA, Shedlock DJ, Jiang J, Troy AE, Shen H. Cutting Edge: CD4 and CD8 T Cells Are Intrinsically Different in Their Proliferative Responses. The Journal of Immunology. 2002;168(4):1528–1532. doi:10.4049/jimmunol.168.4.1528.

79. Lucas ED, Finlon JM, Burchill MA, McCarthy MK, Morrison TE, Colpitts TM, et al. Type 1 IFN and PD-L1 Coordinate Lymphatic Endothelial Cell Expansion and Contraction during an Inflammatory Immune Response. The Journal of Immunology. 2018;201(6):1735–1747. doi:10.4049/jimmunol.1800271.

80. Lucas ED, Tamburini BAJ. Lymph Node Lymphatic Endothelial Cell Expansion and Contraction and the Programming of the Immune Response. Frontiers in Immunology. 2019;10:36. doi:10.3389/fimmu.2019.00036.

81. Adair TH, Guyton AC. Modification of lymph by lymph nodes. II. Effect of increased lymph node venous blood pressure. American Journal of Physiology-Heart and Circulatory Physiology. 1983;245(4):H616–H622. doi:10.1152/ajpheart.1983.245.4.H616.

82. Adair T, Guyton A. Modification of lymph by lymph nodes. III. Effect of increased lymph hydrostatic pressure. The American journal of physiology. 1985;249:H777–82. doi:10.1152/ajpheart.1985.249.4.H777.

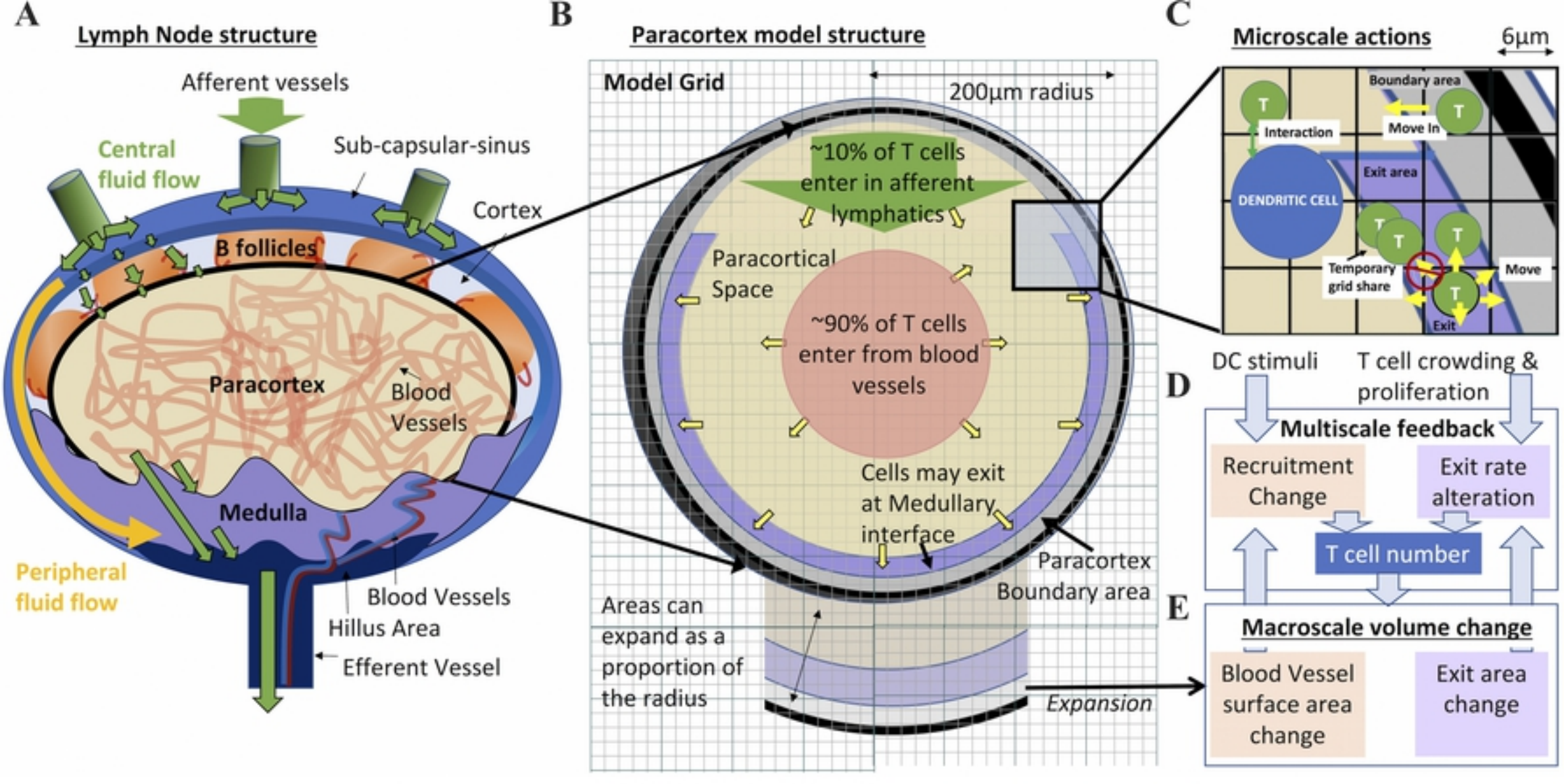
A
Lymph Node structure
Afferent vessels
Central fluid flow
Sub-capsular-sinus
Cortex
B follicles
Paracortex
Blood Vessels
Medulla
Peripheral fluid flow
Blood Vessels
Hillus Area
Efferent Vessel
B
Paracortex model structure
Model Grid
200μm radius
~10% of T cells enter in afferent lymphatics
Paracortical Space
~90% of T cells enter from blood vessels
Cells may exit at Medullary interface
Paracortex Boundary area
Areas can expand as a proportion of the radius
Expansion
C
Microscale actions
6μm
Boundary area
Interaction
Move In
Exit area
DENDRITIC CELL
Temporary grid share
Move
Exit
D
DC stimuli
T cell crowding & proliferation
Multiscale feedback
Recruitment Change
Exit rate alteration
T cell number
E
Macroscale volume change
Blood Vessel surface area change
Exit area change

Figure_1

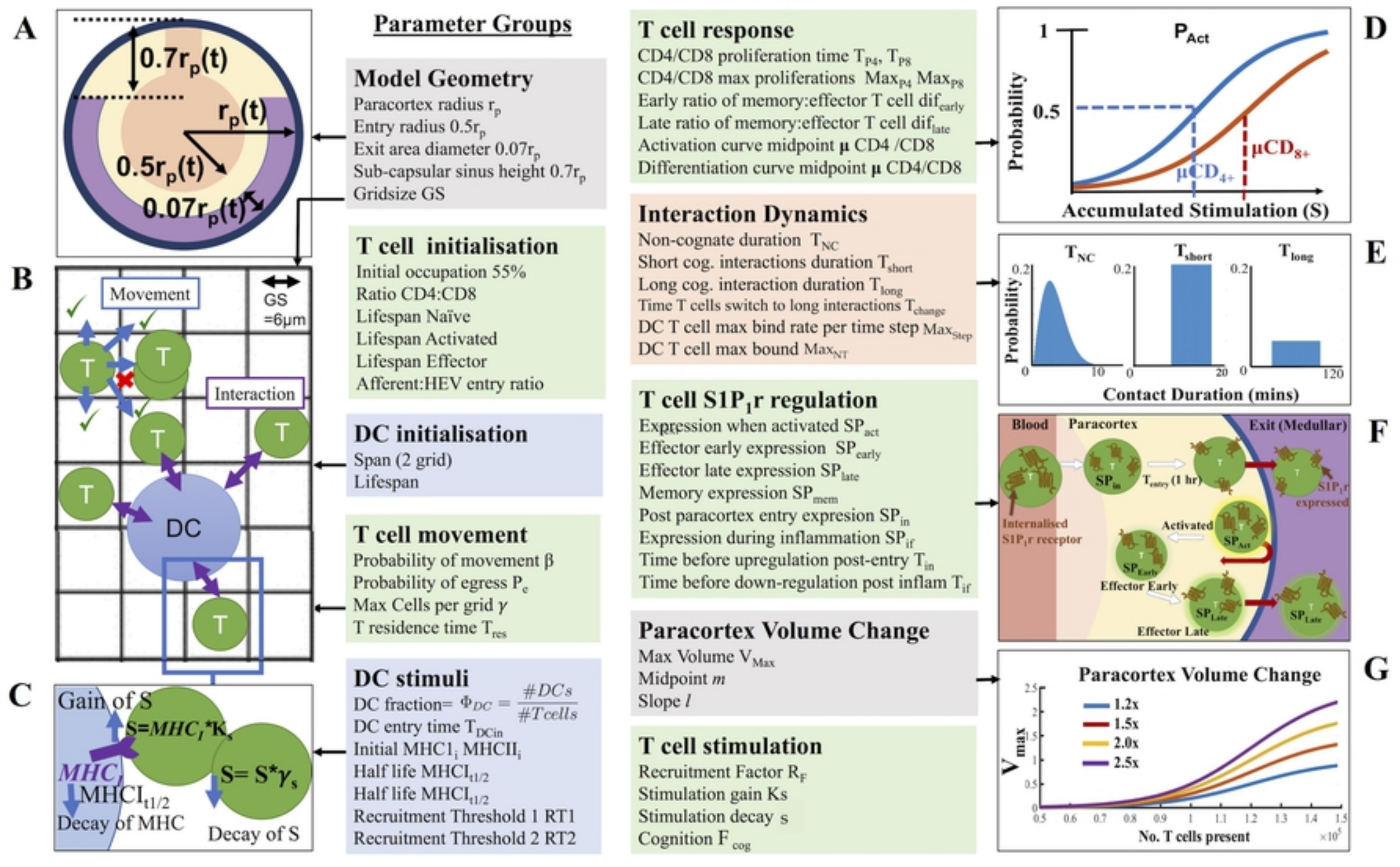
A
B
C
D
E
F
G
Parameter Groups
Model Geometry
Paracortex radius r_p
Entry radius $0.5r_p$
Exit area diameter $0.07r_p$
Sub-capsular sinus height $0.7r_p$
Gridsize GS
T cell initialisation
Initial occupation 55%
Ratio CD4:CD8
Lifespan Naïve
Lifespan Activated
Lifespan Effector
Afferent:HEV entry ratio
DC initialisation
Span (2 grid)
Lifespan
T cell movement
Probability of movement β
Probability of egress P_e
Max Cells per grid γ
T residence time T_{res}
DC stimuli
DC fraction= $\Phi_{DC} = \frac{\#DCs}{\#Tcells}$
DC entry time T_{DCin}
Initial $MHC1_i$ $MHCII_i$
Half life $MHCI_{t1/2}$
Half life $MHCI_{t1/2}$
Recruitment Threshold 1 RT1
Recruitment Threshold 2 RT2
T cell response
CD4/CD8 proliferation time T_{P4}, T_{P8}
CD4/CD8 max proliferations Max_{P4} Max_{P8}
Early ratio of memory:effector T cell dif_{early}
Late ratio of memory:effector T cell dif_{late}
Activation curve midpoint μ CD4 /CD8
Differentiation curve midpoint μ CD4/CD8
Interaction Dynamics
Non-cognate duration T_{NC}
Short cog. interactions duration T_{short}
Long cog. interaction duration T_{long}
Time T cells switch to long interactions T_{change}
DC T cell max bind rate per time step Max_{Step}
DC T cell max bound Max_{NT}
T cell $S1P_1r$ regulation
Expression when activated SP_{act}
Effector early expression SP_{early}
Effector late expression SP_{late}
Memory expression SP_{mem}
Post paracortex entry expresion SP_{in}
Expression during inflammation SP_{if}
Time before upregulation post-entry T_{in}
Time before down-regulation post inflam T_{if}
Paracortex Volume Change
Max Volume V_{Max}
Midpoint m
Slope l
T cell stimulation
Recruitment Factor R_F
Stimulation gain Ks
Stimulation decay s
Cognition F_{cog}
Movement
GS =6μm
Interaction
DC
Gain of S
$S=MHC_I*K_s$
MHC_I
$MHCI_{t1/2}$
Decay of MHC
$S= S*\gamma_s$
Decay of S
Probability
Accumulated Stimulation (S)
P_{Act}
μCD4+
μCD8+
T_{NC}
T_{short}
T_{long}
Contact Duration (mins)
Blood
Paracortex
Exit (Medullar)
Internalised $S1P_1r$ receptor
T_{entry} (1 hr)
$S1P_1r$ expressed
Activated
Effector Early
Effector Late
Paracortex Volume Change
1.2x
1.5x
2.0x
2.5x
V_{max}
No. T cells present

Figure_2

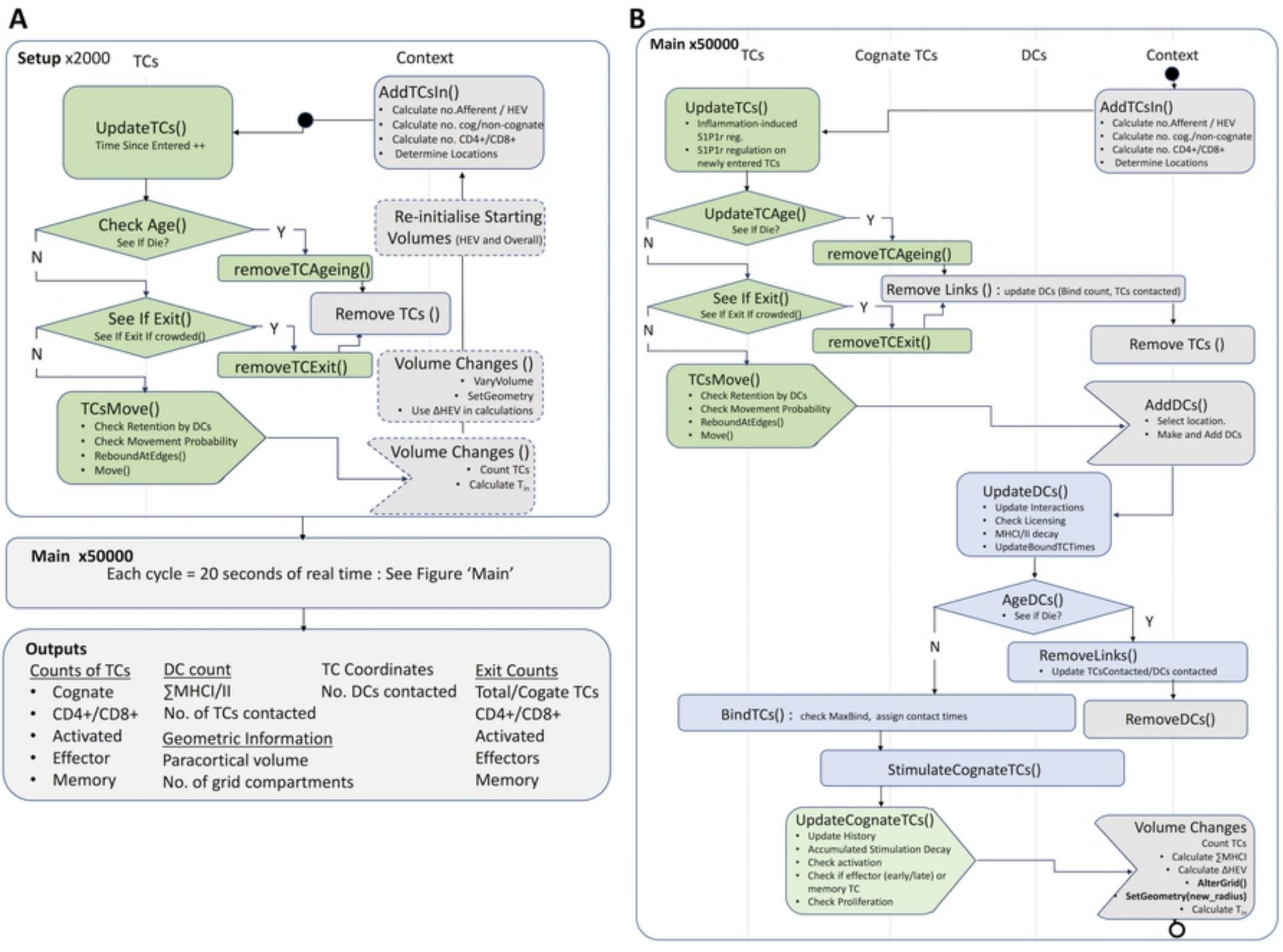
A
Setup x2000
TCs
Context
UpdateTCs()
Time Since Entered ++
AddTCsIn()
Calculate no.Afferent / HEV
Calculate no. cog/non-cognate
Calculate no. CD4+/CD8+
Determine Locations
Check Age()
See If Die?
Y
N
removeTCAgeing()
Re-initialise Starting Volumes (HEV and Overall)
See If Exit()
See If Exit If crowded()
Y
N
removeTCExit()
Remove TCs ()
Volume Changes ()
VaryVolume
SetGeometry
Use ΔHEV in calculations
TCsMove()
Check Retention by DCs
Check Movement Probability
ReboundAtEdges()
Move()
Volume Changes ()
Count TCs
Calculate T_{in}
Main x50000
Each cycle = 20 seconds of real time : See Figure 'Main'
Outputs
Counts of TCs
Cognate
CD4+/CD8+
Activated
Effector
Memory
DC count
∑MHCI/II
No. of TCs contacted
Geometric Information
Paracortical volume
No. of grid compartments
TC Coordinates
No. DCs contacted
Exit Counts
Total/Cogate TCs
CD4+/CD8+
Activated
Effectors
Memory
B
Main x50000
TCs
Cognate TCs
DCs
Context
UpdateTCs()
Inflammation-induced S1P1r reg.
S1P1r regulation on newly entered TCs
AddTCsIn()
Calculate no.Afferent / HEV
Calculate no. cog./non-cognate
Calculate no. CD4+/CD8+
Determine Locations
UpdateTCAge()
See If Die?
Y
N
removeTCAgeing()
Remove Links () : update DCs (Bind count, TCs contacted)
See If Exit()
See If Exit If crowded()
Y
N
removeTCExit()
Remove TCs ()
TCsMove()
Check Retention by DCs
Check Movement Probability
ReboundAtEdges()
Move()
AddDCs()
Select location.
Make and Add DCs
UpdateDCs()
Update Interactions
Check Licensing
MHCI/II decay
UpdateBoundTCTimes
AgeDCs()
See if Die?
N
Y
RemoveLinks()
Update TCsContacted/DCs contacted
BindTCs() : check MaxBind, assign contact times
RemoveDCs()
StimulateCognateTCs()
UpdateCognateTCs()
Update History
Accumulated Stimulation Decay
Check activation
Check if effector (early/late) or memory TC
Check Proliferation
Volume Changes
Count TCs
Calculate ∑MHCI
Calculate ΔHEV
AlterGrid()
SetGeometry(new_radius)
Calculate T_{in}

Figure_3

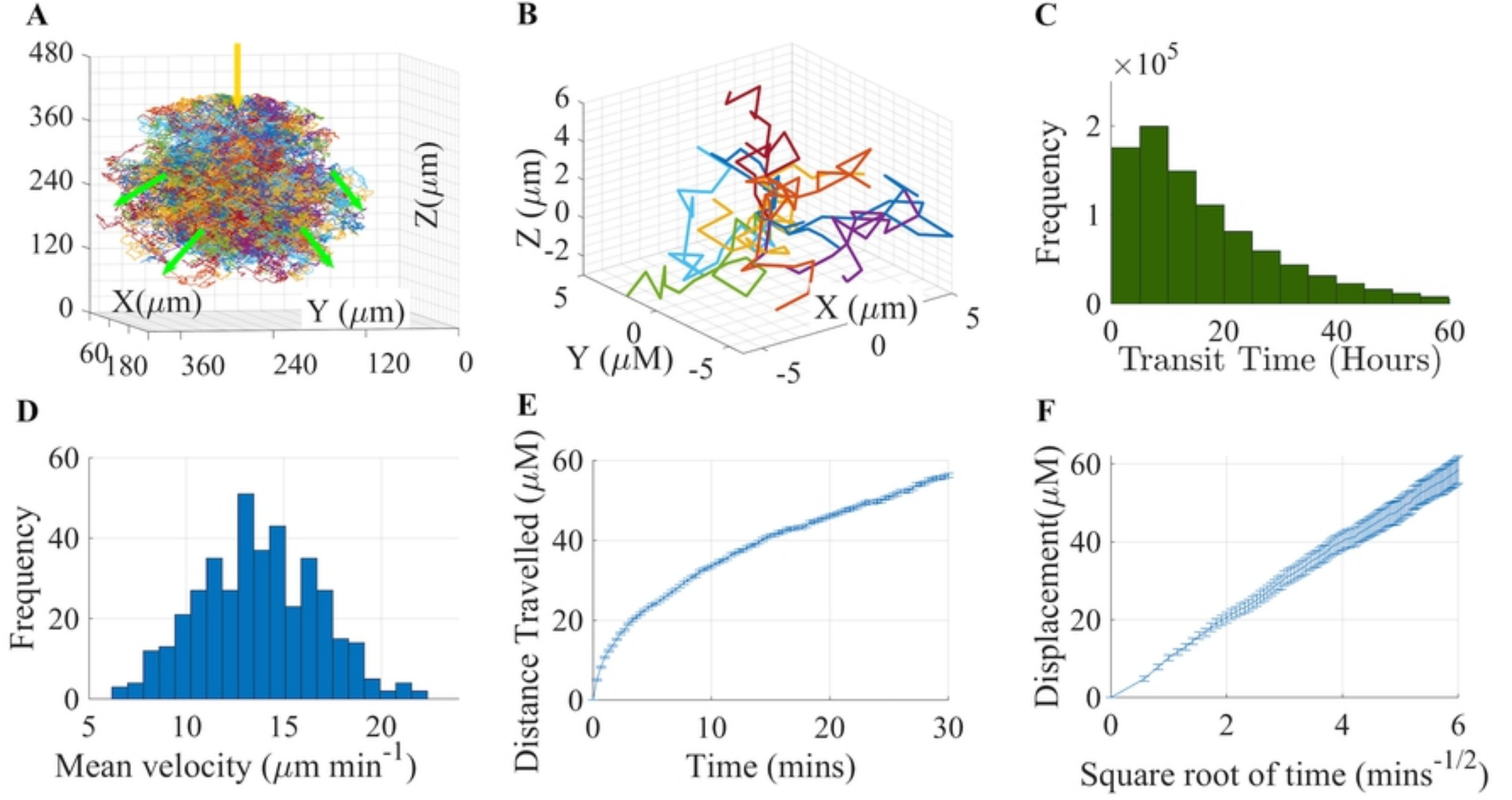
A
480
360
240
120
0
X(μm)
Y (μm)
Z(μm)
60
180
360
240
120
0
B
Z (μm)
6
4
2
0
-2
5
0
Y (μM)
-5
X (μm)
5
0
-5
C
×10^5
Frequency
2
1
0
0
20
40
60
Transit Time (Hours)
D
Frequency
60
40
20
0
5
10
15
20
Mean velocity (μm min^-1)
E
Distance Travelled (μM)
60
40
20
0
0
10
20
30
Time (mins)
F
Displacement(μM)
60
40
20
0
0
2
4
6
Square root of time (mins^-1/2)

Figure_4

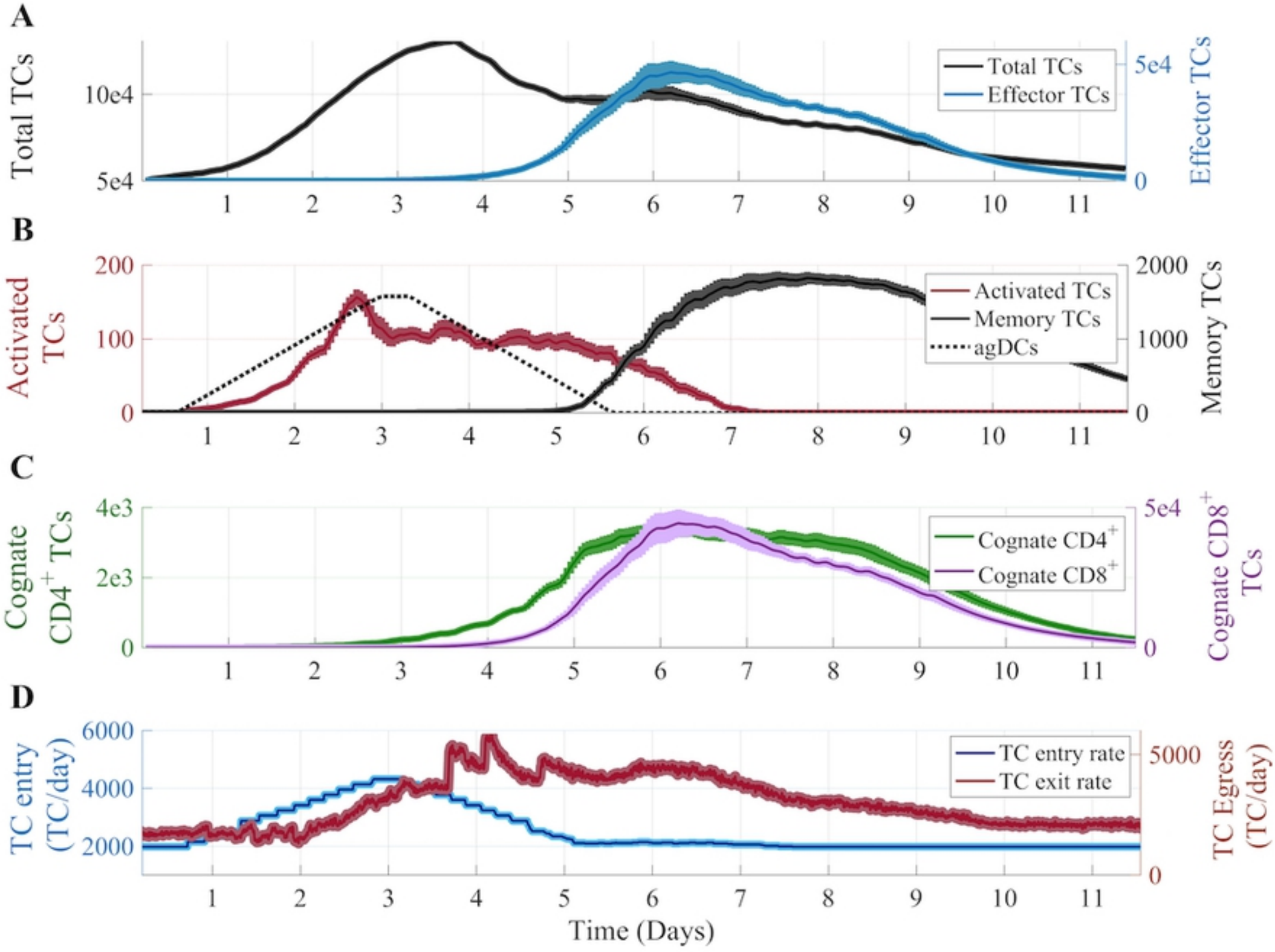
A
Total TCs
10e4
5e4
Effector TCs
5e4
0
Total TCs
Effector TCs
1
2
3
4
5
6
7
8
9
10
11
B
Activated TCs
200
100
0
Memory TCs
2000
1000
0
Activated TCs
Memory TCs
agDCs
C
Cognate CD4+ TCs
4e3
2e3
0
Cognate CD8+ TCs
5e4
0
Cognate CD4+
Cognate CD8+
D
TC entry (TC/day)
6000
4000
2000
TC Egress (TC/day)
5000
0
TC entry rate
TC exit rate
Time (Days)

Figure_5

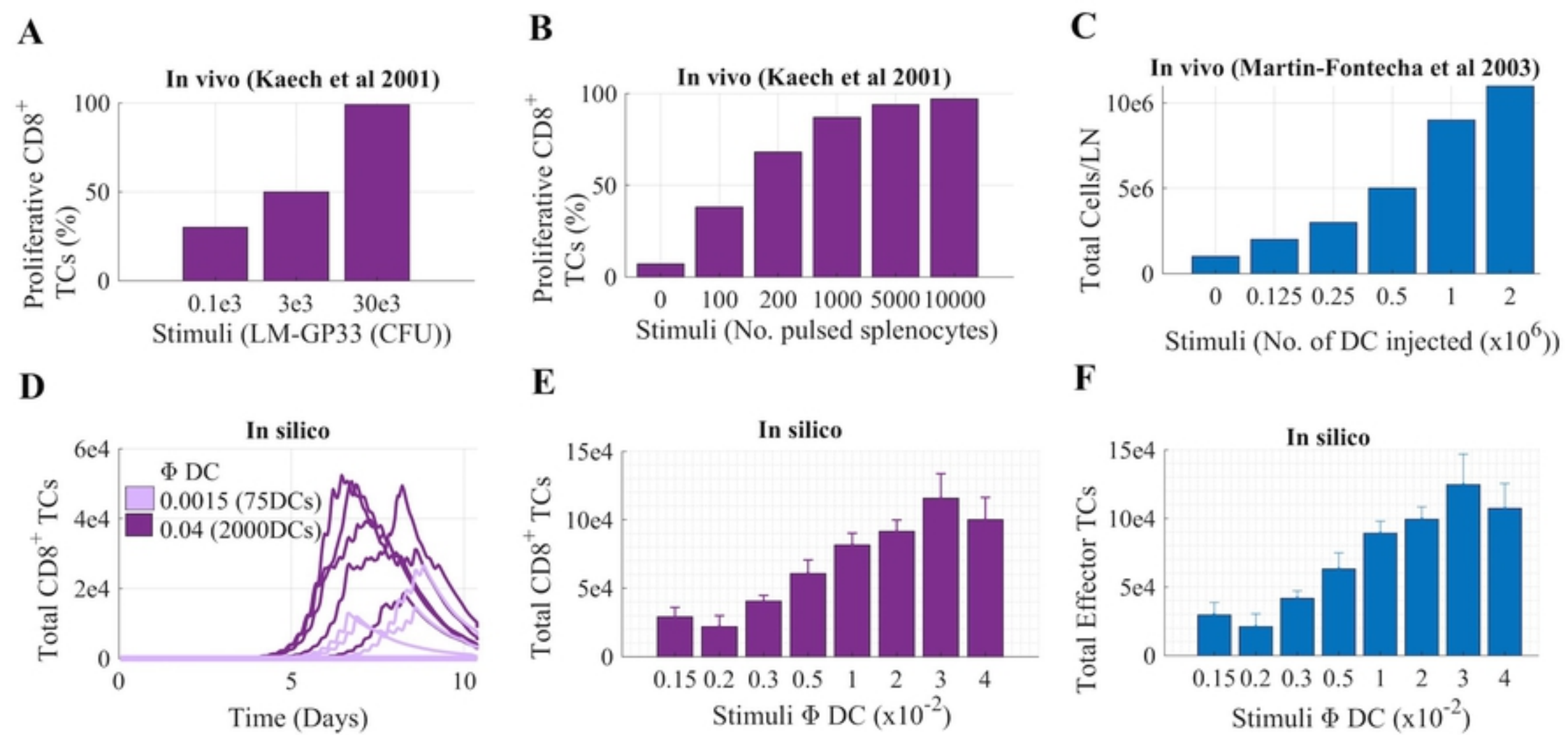
A
In vivo (Kaech et al 2001)
Proliferative CD8+ TCs (%)
100
50
0
0.1e3
3e3
30e3
Stimuli (LM-GP33 (CFU))
B
In vivo (Kaech et al 2001)
Proliferative CD8+ TCs (%)
100
50
0
0
100
200
1000
5000
10000
Stimuli (No. pulsed splenocytes)
C
In vivo (Martin-Fontecha et al 2003)
Total Cells/LN
10e6
5e6
0
0
0.125
0.25
0.5
1
2
Stimuli (No. of DC injected (x10^6))
D
In silico
Total CD8+ TCs
6e4
4e4
2e4
0
Φ DC
0.0015 (75DCs)
0.04 (2000DCs)
0
5
10
Time (Days)
E
In silico
Total CD8+ TCs
15e4
10e4
5e4
0
0.15
0.2
0.3
0.5
1
2
3
4
Stimuli Φ DC (x10^-2)
F
In silico
Total Effector TCs
15e4
10e4
5e4
0
0.15
0.2
0.3
0.5
1
2
3
4
Stimuli Φ DC (x10^-2)

Figure_6

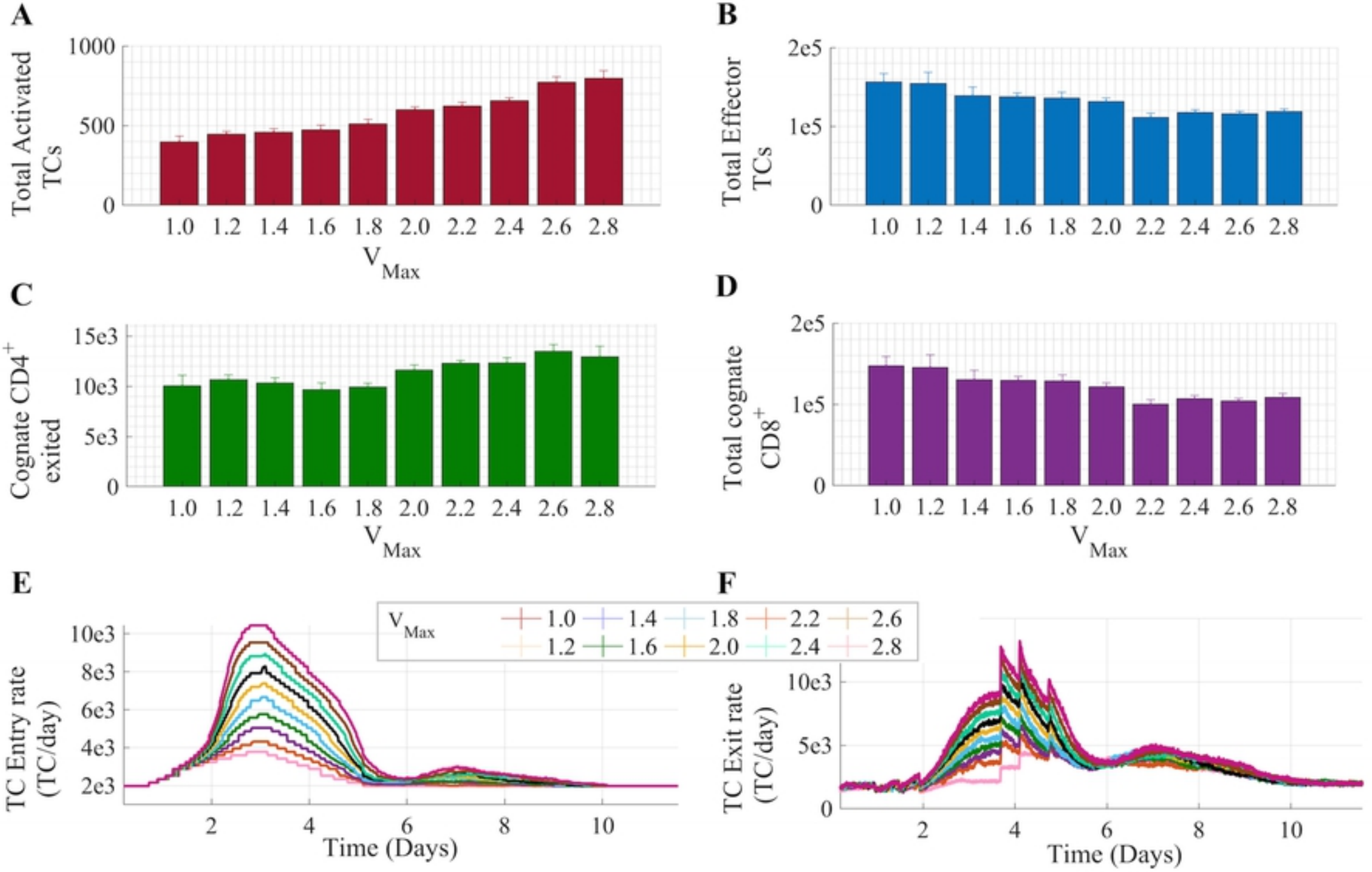
A
Total Activated TCs
1000
500
0
1.0 1.2 1.4 1.6 1.8 2.0 2.2 2.4 2.6 2.8
V Max
B
Total Effector TCs
2e5
1e5
0
1.0 1.2 1.4 1.6 1.8 2.0 2.2 2.4 2.6 2.8
C
Cognate CD4+ exited
15e3
10e3
5e3
0
1.0 1.2 1.4 1.6 1.8 2.0 2.2 2.4 2.6 2.8
V Max
D
Total cognate CD8+
2e5
1e5
0
1.0 1.2 1.4 1.6 1.8 2.0 2.2 2.4 2.6 2.8
V Max
E
V Max
1.0 1.2 1.4 1.6 1.8 2.0 2.2 2.4 2.6 2.8
TC Entry rate (TC/day)
10e3
8e3
6e3
4e3
2e3
2 4 6 8 10
Time (Days)
F
TC Exit rate (TC/day)
10e3
5e3
0
2 4 6 8 10
Time (Days)

Figure_7

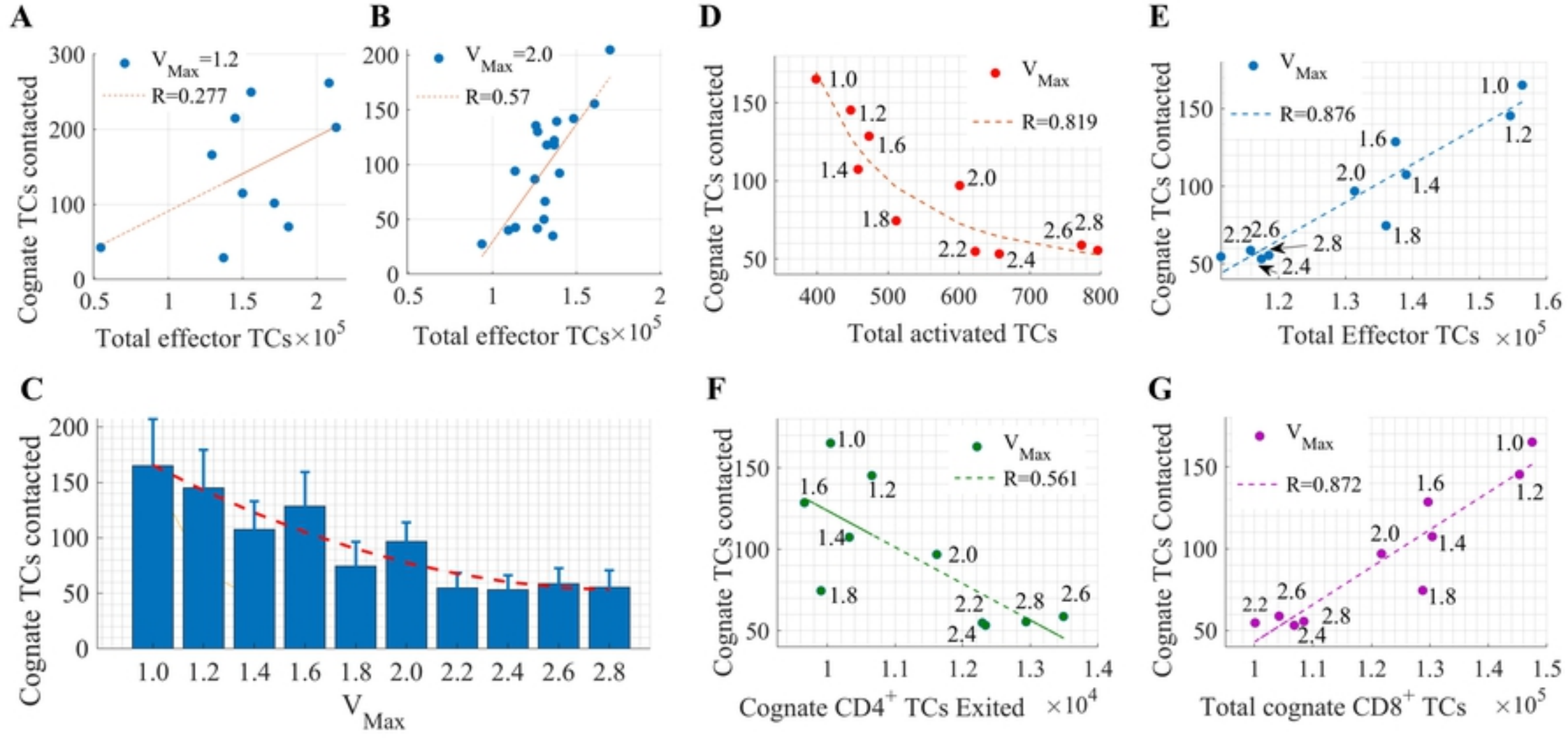
A
B
C
D
E
F
G
Cognate TCs contacted
Total effector TCs×10^5
V_Max=1.2
R=0.277
V_Max=2.0
R=0.57
V_Max
Total activated TCs
R=0.819
Cognate TCs Contacted
Total Effector TCs ×10^5
R=0.876
Cognate CD4+ TCs Exited ×10^4
R=0.561
Total cognate CD8+ TCs ×10^5
R=0.872

Figure_8

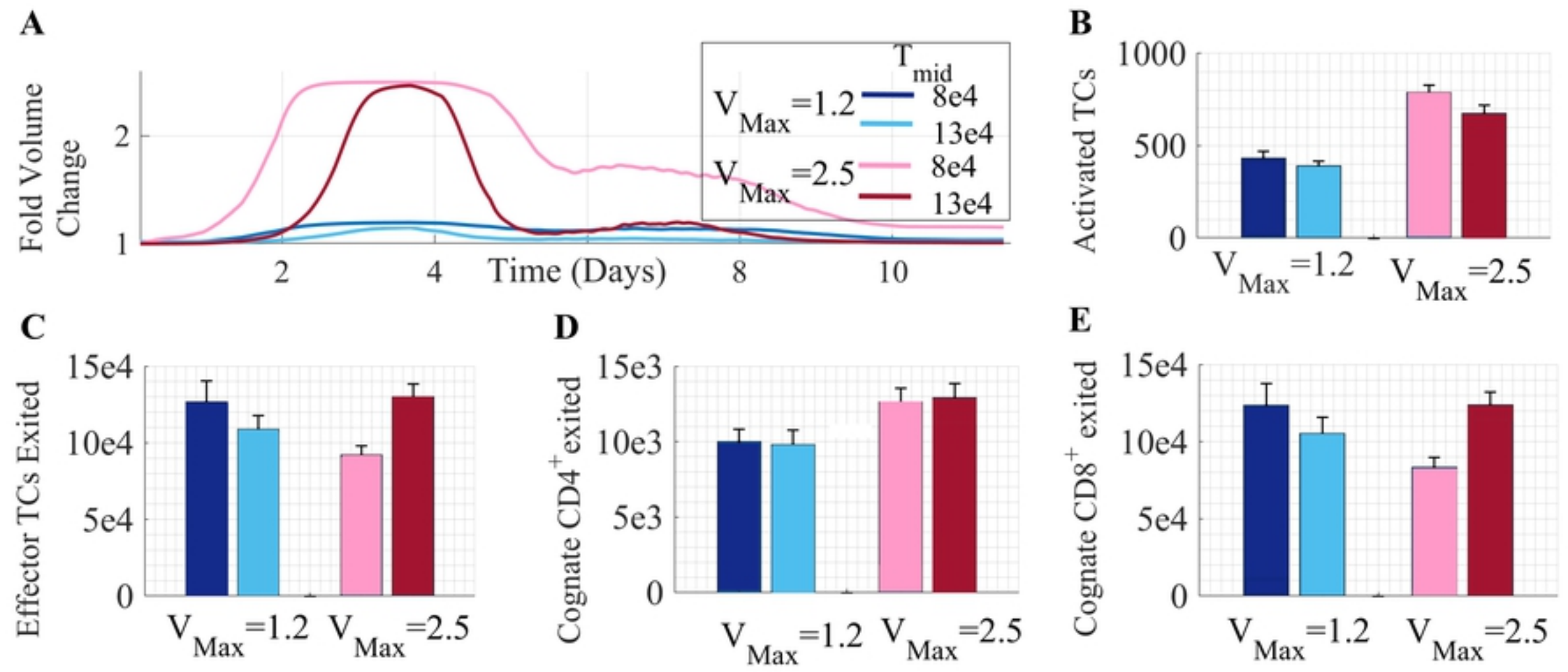
A
Fold Volume Change
2
1
2
4
Time (Days)
8
10
T mid
V Max =1.2
8e4
13e4
V Max =2.5
8e4
13e4
B
Activated TCs
1000
500
0
V Max =1.2
V Max =2.5
C
Effector TCs Exited
15e4
10e4
5e4
0
V Max =1.2
V Max =2.5
D
Cognate CD4+ exited
15e3
10e3
5e3
0
V Max =1.2
V Max =2.5
E
Cognate CD8+ exited
15e4
10e4
5e4
0
V Max =1.2
V Max =2.5

Figure_9

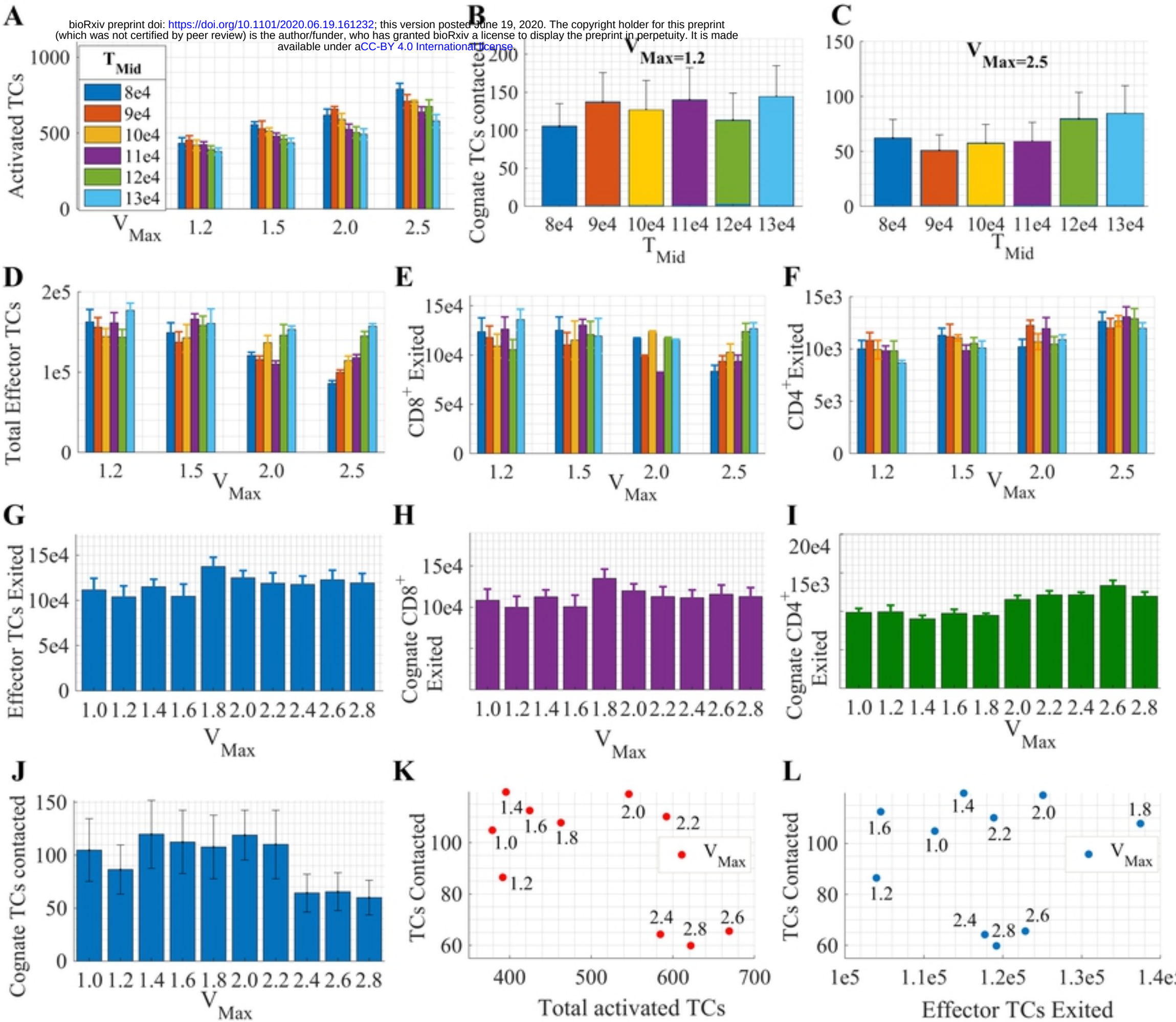

Figure_10

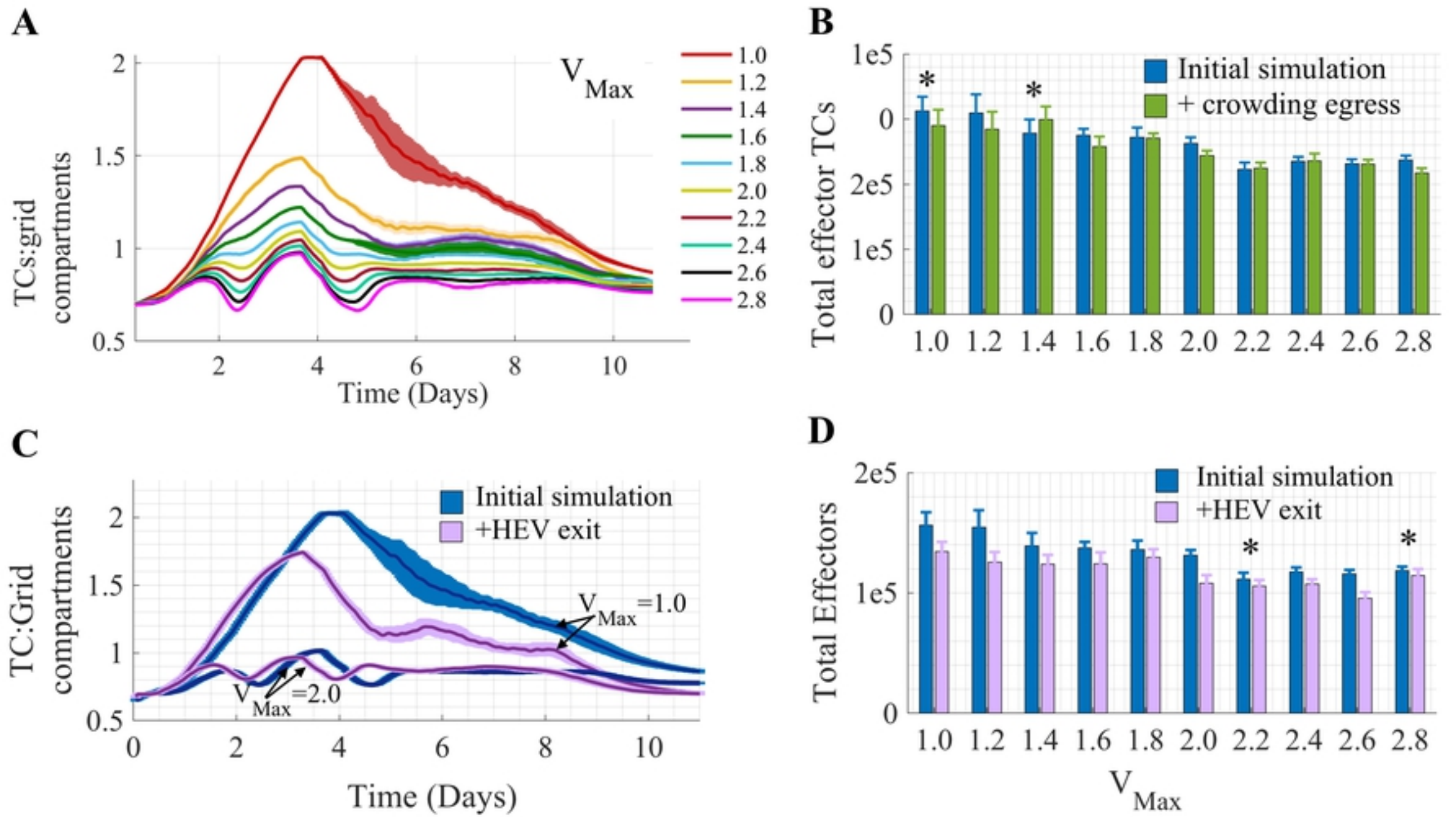
A
TCs:grid compartments
Time (Days)
V Max
1.0
1.2
1.4
1.6
1.8
2.0
2.2
2.4
2.6
2.8
B
Total effector TCs
Initial simulation
+ crowding egress
C
TC:Grid compartments
Initial simulation
+HEV exit
V Max =1.0
V Max =2.0
Time (Days)
D
Total Effectors
Initial simulation
+HEV exit
V Max

Figure_11

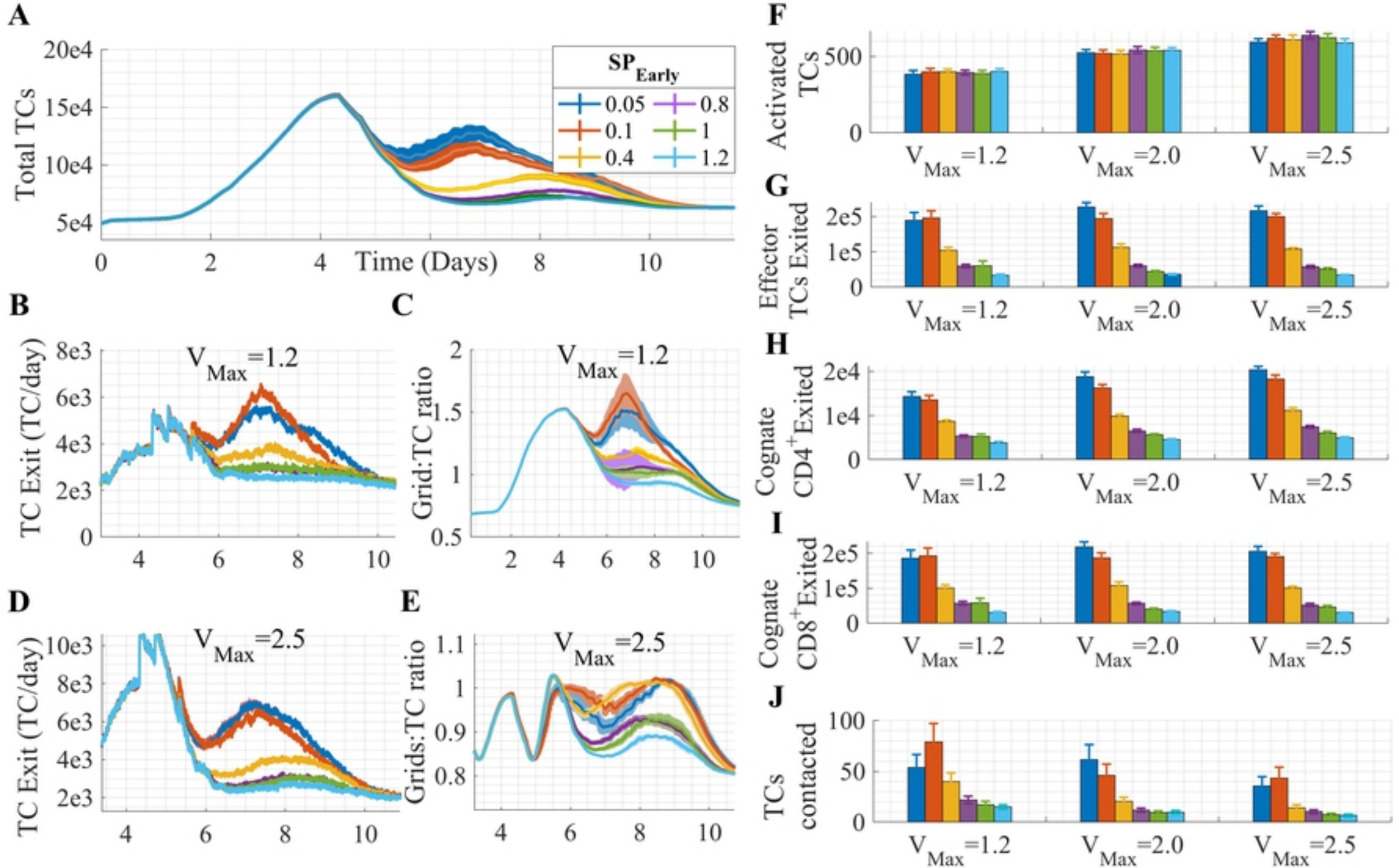
A
Total TCs
20e4
15e4
10e4
5e4
0
2
4
Time (Days)
8
10
SP Early
0.05
0.8
0.1
1
0.4
1.2
B
TC Exit (TC/day)
8e3
6e3
4e3
2e3
0
V Max =1.2
4
6
8
10
C
Grid:TC ratio
2
1.5
1
0.5
V Max =1.2
2
4
6
8
10
D
TC Exit (TC/day)
10e3
8e3
6e3
4e3
2e3
V Max =2.5
4
6
8
10
E
Grids:TC ratio
1.1
1
0.9
0.8
V Max =2.5
4
6
8
10
F
Activated TCs
500
0
V Max =1.2
V Max =2.0
V Max =2.5
G
Effector TCs Exited
2e5
1e5
0
V Max =1.2
V Max =2.0
V Max =2.5
H
Cognate CD4+ Exited
2e4
1e4
0
V Max =1.2
V Max =2.0
V Max =2.5
I
Cognate CD8+ Exited
2e5
1e5
0
V Max =1.2
V Max =2.0
V Max =2.5
J
TCs contacted
100
50
0
V Max =1.2
V Max =2.0
V Max =2.5

Figure_12